Batteries & Supercaps

Review
doi.org/10.1002/batt.202200328

Chemistry Europe
European Chemical Societies Publishing

www.batteries-supercaps.org

Current Status of Formulations and Scalable Processes for Producing Sulfidic Solid-State Batteries

Mattis Batzer[+],*[a] Carina Heck[+],[a] Peter Michalowski,[a] and Arno Kwade[a]

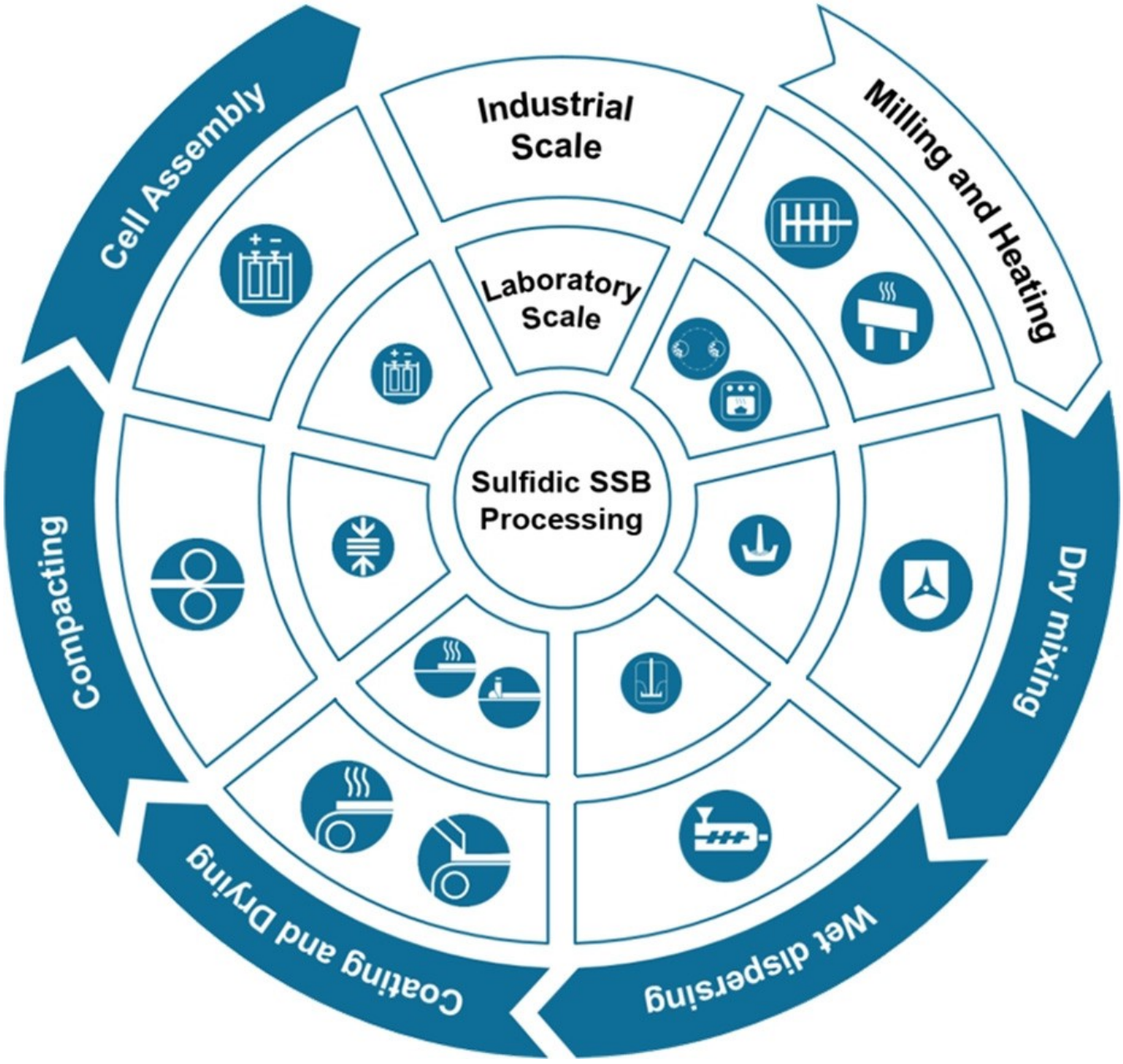

Solid-state batteries possess the potential to combine increased energy densities, high voltages, as well as safe operation and therefore are considered the future technology for electrical energy storage. In particular, sulfides as solid electrolyte are promising candidates due to their high ionic conductivities and the possibility of a scalable production. This review aims to demonstrate ways to manufacture suspension-based sulfidic solid-state batteries both on a laboratory scale and on an industrial level, focusing on the assessment of current knowledge and its discussion from a process engineering point of view. In addition to the influence of process parameters during mechanochemical synthesis of the solid electrolyte, formulation strategies for electrodes and separators are presented. The process chain from dispersion to cell assembly is evaluated. Scale-up technologies are considered in comparison to established techniques in the field of conventional lithium-ion batteries with liquid electrolyte summarizing the current status of sulfidic solid-state battery production.

1. Introduction

1.1. Advantages and challenges compared to conventional LIBs

Initiating the energy transition – moving from fossil fuels to renewable energy sources – requires the development of innovative storage technologies that can compensate the temporary discrepancies between the production and consumption of energy.[1] While performance gains in conventional lithium-ion batteries (LIB) will not reach the level of fossil fuels in the near future,[2] a new promising technology is now entering the field in the shape of the solid-state battery (SSB). The most obvious advantage results from the substitution of the liquid electrolyte by a solid: leakage of the flammable and explosive fluid is no longer possible, which increases the safety of the cell.[1,3–7] As a result, a cooling system to prevent ignition is also obsolete, which favors the energy density of the battery by reducing the necessary periphery.[1] Although there is a temperature dependence of the ionic conductivity especially for polymer solid electrolytes (SE),[8] freezing or boiling of the electrolyte do not play a role, which makes the SSB less temperature-sensitive than its conventional predecessors.[9,10] Other elements that positively influence the energy density result from the chemical stability of some SEs: In addition to the possibility of using pure lithium or lithium free disposition structures as the anode,[11,12] a high voltage can be applied to SSBs due to the lack of dissociation of the electrolyte.[13,14] Series connection of the battery cells (bipolar stacking) is possible and results in an increased cell voltage, as well as savings in current collectors.[1] Very long cycle lifes complete the profile of SSBs.[9,11,15] The latter can be achieved by using fiber-reinforced, structurally integrated battery materials, giving the cells a load-bearing function in addition to their primary task of storing energy. This leads to a substitution of other materials, which results in weight savings making even aerospace applications viable.

1.2. Structure and function

Figure 1 schematically shows the structure of a SSB in discharge state. While the cathode is applied in the form of a particulate layer on aluminum, different anode concepts can be used: In the long term and for a large scale, the application of metallic lithium is desired,[12] which enables the above mentioned advantages and is financially affordable on a large scale. Currently, on a laboratory-scale indium or lithium-indium are common, which is easier to handle and obtain more reproducible results. However, indium is not suitable for scaling due to its lower abundance and thus high cost. Also possible is the deposition of lithium. For metallic lithium or indium, copper serves as the current collector.[16] Alternatively, the anode can be produced similar to the cathode based on particulate material. In this case, however, stainless steel is used as the current collector[11] because of possible reaction between solid electrolyte and current collector. The most important ingredient of such particulate electrodes is the active material in which lithium ions can be stored. Conversion type active materials, such as sulfur, could be an interesting alternative, but are still in an early stage of development.[17] In this case, the large volume change poses a major challenge. In addition, binders are required to ensure mechanical integrity, conductive additives for electron conduction and SEs for ion conductivity. The electrodes are isolated from each other by a separator composed of SE particles and binder. It maintains electrical isolation and high ionic conductivity.

1.3. Requirements, structure and properties of SEs

To carry out their function, a number of requirements have to be fulfilled by the SEs: In addition to high ionic conductivity and electrical insulation of the electrode layers, (electro-) chemical stability with respect to both the other cell components (e.g., active materials, conductive additives). This must be maintained over the entire voltage window to keep side reactions and degradation low. Furthermore, high mechanical stability and elasticity are required to be able to ensure scalable production processes such as roll-to-roll coating and to maintain the

[a] M. Batzer,[+] C. Heck,[+] Dr. P. Michalowski, Prof. Dr. A. Kwade
Institut für Partikeltechnik
Technische Universität Braunschweig
Volkmaroder Str. 5, 38104 Braunschweig, Germany
E-mail: m.batzer@tu-braunschweig.de
Homepage: www.ipat.tu-braunschweig.de
[+] These authors contribute equality to this work.

Review
doi.org/10.1002/batt.202200328
Chemistry Europe
European Chemical Societies Publishing

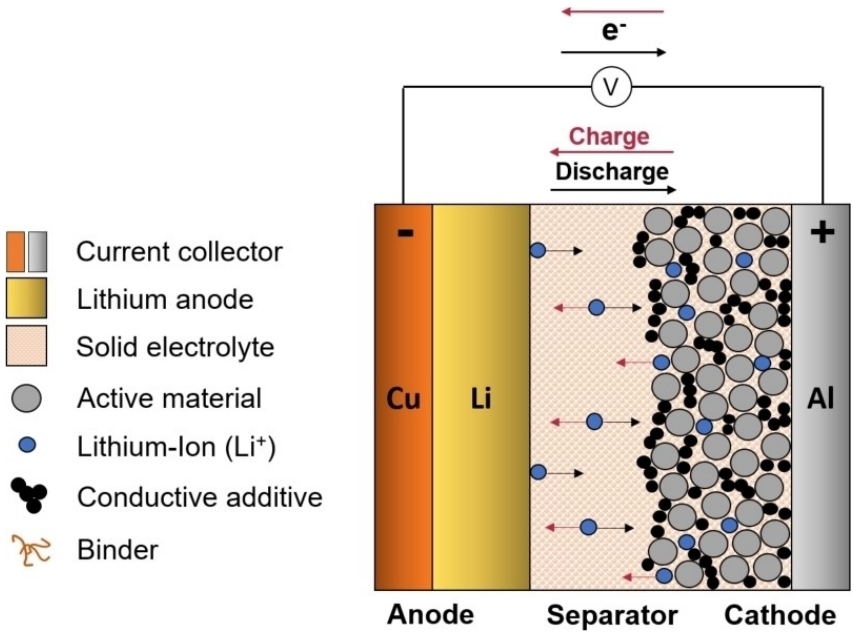

Figure 1. Schematic illustration of an SSB.

mechanical integrity of the cell even when the cell is in operation (due to volume change during the intercalation process, dendrite formation). In addition, there are economic requirements such as the availability of the materials and low costs for a cost-efficient implementation on an industrial scale.

SEs can be divided into organic and inorganic ones. They differ in terms of chemical, mechanical and electrochemical properties: In general, organic SEs (e.g., polymers) are comparatively easy to process, but have poor ionic conductivity at room temperature and are thermally and chemically unstable with respect to other components when exposed to temperature fluctuations. Inorganic SEs (e.g., sulfides, oxides), on the other hand, exhibit comparably high ionic conductivities even at ambient temperature, but are more complex to process. Examples include the sensitivity of sulfides to moisture, which requires processing in gloveboxes under inert gas or at least dry

M. Sc. Mattis Batzer has studied mechanical engineering at Technische Universität Braunschweig and is a research associate and PhD student at the Institute of Particle Technology since 2018. Besides publishing systematic cathode and separator formulation studies for sulfide-based solid-state batteries, he established a process route for their scalable production including a twin-screw extruder. Since 2022, he is head of the working group "Component" of the Battery LabFactory Braunschweig, which deals with innovative lithium-ion and solid-state batteries.

M. Sc. Carina Amata Heck has studied biotechnology from 2014 to 2019 at the Technische Universität Braunschweig and is a research associate and PhD student at the Institute of Particle Technology since 2020 under the supervision of Prof. Dr.-Ing. Arno Kwade. Next to her considerations of nickel-rich cathode active materials for conventional lithium-ion batteries her research focus lays on the densification process of sulfide-based composite cathodes and separators for solid state batteries.

Dr. rer. nat. Peter Michalowski has studied physics at the Friedrich-Schiller-Universität Jena and University of Uppsala. In 2017 he received his doctoral degree at the Carl von Ossietzky Universität Oldenburg on spinel thin film cathodes. Since 2019 he leads the junior research group "Solid-State Battery Materials and Electrodes" and since 2021 he is the head of the battery engineering devision at the Institute of Particle Technology of the Technische Universität Braunschweig.

Prof. Dr.-Ing. Arno Kwade studied mechanical engineering from 1986 to 1992 at the Technische Universität Braunschweig and the University of Waterloo. After finishing his PhD in 1996 on ultrafine milling processes and working as a general manager and executive director for 9 years in industry, he became a full professor and head of the Institute for Particle Technology of the TU Braunschweig in 2005. Here, particle-related questions in the field of battery process engineering and pharmaceutics are considered. He is also chairman of the Battery LabFactory Braunschweig (BLB) and the Center for Pharmaceutical Process Engineering at TU Braunschweig (PVZ).

room atmospheres with very low dew points, or the high temperatures necessary for sintering oxides.[11] Due to the focus on sulfidic SEs in this work, only those will be considered in the following. As examples of some sulfidic SEs, three of each class (thiophosphates, halide argyrodites, sulfides without phosphorous, sulfidic glasses)[18] and their ionic conductivities are given below in Table 1. Since the conductivity of a SE pellet depends on many parameters such as manufacturing and operating pressure,[19] as well as measuring temperature or particle size, these values can fluctuate considerably.[20]

2. Challenges of Sulfide Electrolytes

In addition to the above-mentioned advantages of sulfidic SSBs, there are some challenges with respect to processing and electrochemical performance that still prevent a full-scale commercialization.[12]

2.1. Reactivity of sulfides and process atmosphere

One of the main challenges with respect to safety and battery performance is the high reactivity of the sulfidic electrolytes. Contact with moisture promotes an electrolyte decomposition and a release of hydrogen sulfide (H_2S), a toxic[40,41] and inflammable gas.[42] Due to their high reactivity to moisture,[43–45] sulfidic electrolytes are usually handled in gloveboxes with inert, dry atmosphere.[1] Rare studies also report a cathode and separator processing in dry room or microenvironments with a dew point below −50 °C, which is aimed because of the easier handling and lower costs.[11,46] Sulfidic electrolytes are usually composed of tetrahedral MS_4 units, where M is typically a Group 14 or Group 15 element.[47] As it is described for Li_2S–P_2S_5, the moisture sensitivity of the sulfidic electrolytes is caused by the preference of the central atom in the MS_4 unit to form a bond with oxygen rather than to sulfur resulting in the formation of both an OH and a SH group bound to the central atom.[47,48] The SH group is subsequently hydrolyzed to another OH group and H_2S is released.[48] Development of sulfidic electrolytes that are more resistant to moisture is always a tradeoff with the ionic conductivity of these materials, as the MS_4 unit is integral to the ion conductive properties of these electrolytes.[47] Potential solutions might be a substitution of sulfur with oxygen, or to use Sn^{4+} and Sb^{5+} as the central cation or dopants. However, these would be quite expensive and unfavorable with regard to energy density in comparison to a phosphorus substitution.[31,47,49] Another approach is to use metal oxides of the type M_xO_y as H_2S adsorbent additives.[47,50] This way, Hayashi et al. synthesized a $90Li_3PS_4$–10ZnO electrolyte with an ionic conductivity of 0.3 mS cm^{-1}.[50] As demonstrated by Muramatsu et al. the composition of Li_2S–P_2S_5 electrolytes can affect the extent to which H_2S is released from the different materials upon their exposure to moisture.[48]

Gassing behavior may occur, not only upon exposure of these electrolytes to moisture, but sometimes also during cycling of the SSB cell. Similar gassing behavior to conventional LIBs with liquid electrolyte has been observed within a sulfidic SSB when $Li_2Ni_xCo_yMn_zO_2$ (NCM) cathode active material is used. A release of O_2 from the bulk and CO_2 from carbonate species or rather protective layers at potentials above 4.5 V with respect to Li^+/Li for pellet-type cells with a $Li_2Ni_{0.6}Co_{0.2}Mn_{0.2}O_2$ (NCM 622) cathode, β-Li_3PS_4 as electrolyte and indium as anode has been reported.[51] In correlation to the release of O_2 an evolution of SO_2 in the indium anode cell has been measured, which verifies a decomposition of the electrolyte. H_2S evolution has never been detected.[51] Furthermore, Walther et al. describe a decomposition of the SE within a Li | β-Li_3PS_4 | NCM 622 | β-Li_3PS_4 pellet-type cell with 2.9 wt% vapor grown carbon fibers (VGCF) by the current collector, the active material, as well as the carbon-based conductive additive.[52] Apart from this, the high reactivity of sulfidic electrolyte requires adaption beyond processing like an appropriate extinguishing media instead of water to minimize the formation of H_2S in case of fire.

Table 1. Selection of sulfidic SEs, their subclasses and ionic conductivities.

Subclass	Composition	Ionic conductivity [mS cm^{-1}]	References
Thiophosphates	$Li_{11}AlP_2S_{12}$	0.80	[21]
	$Li_7P_3S_{11}$	3.20–5.20	[22, 23]
	$Li_{10}GeP_2S_{12}$	6.20–12.00	[24, 25]
Halide argyrodites	Li_6PS_5I	0.19–1.10	[26–28]
	Li_6PS_5Cl	1.33	[26]
	Li_6PS_5Br	0.62–2.58	[26, 29]
Sulfides without phosphorous	Li_2SnS_3	0.02–1.60	[30]
	Li_4SnS_4	0.07–3.00	[31, 32]
	$60Li_2S$–$40SiS_2$	0.15	[33]
Glassy sulfides	Li_3PS_4	0.20–1.00	[24, 34, 35]
	$78Li_2S$–$22P_2S_5$	0.85–1.78	[36, 37]
	$Li_{10}SnP_2S_{12}$	4.00	[38, 39]

2.2. Contact loss caused by chemo-mechanical contraction

During charging/discharging of the cell, cathode active material's, such as lithium cobalt oxide or NCM undergo reversible lattice volume changes within their crystal structure.[53] Because the SE cannot flow or infiltrate the active materials pores like a liquid electrolyte, this results in a loss of contact between the active material and the SE, due to the reversible volume changes of the active material (see Figure 2) which increases the interfacial resistance and capacity loss.[54] The delithiation during charging usually causes a shrinkage of the active material.[53] The volume expansion of $LiCoO_2$ during charging is one rare exception here.[53,55]

One study also reports a quasi-zero-strain NCM material due to a high cobalt content.[56] However, with respect to capacity, material costs and mining conditions a higher nickel content seems to be favorable.[57] In this context, it is assumed that different NCM particle sizes are associated with different chemo-mechanical effects during cycling, which can result in different dimensions of contact loss to the electrolyte.[58] Strauss et al. tested three NCM 622 with different particle sizes (d_{50} = 15.6 μm, 8.3 μm and 4.0 μm) in combination with nanoporous β-Li_3PS_4 in

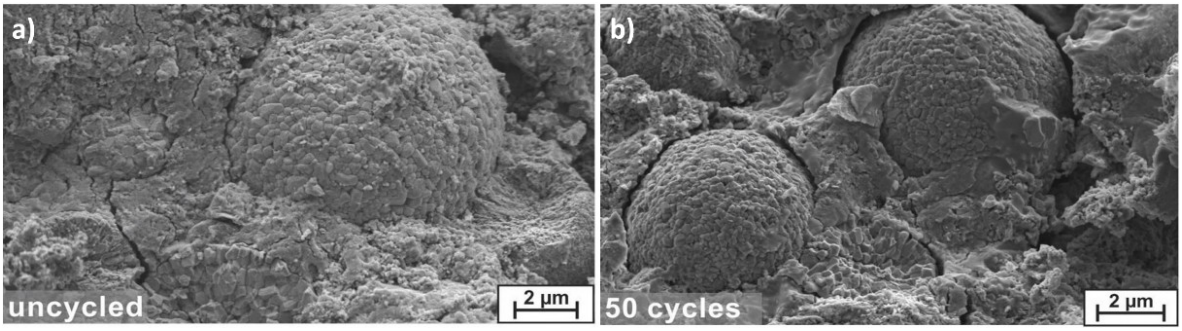

Figure 2. Scanning electron micrographs of a composite cathode within a Li-In I β-Li_3PS_4 I NCM 811 + Li_3PS_4 cell. a) Uncycled state b) after 50 cycles in discharged state (after rate test at 0.1 C, 0.25 C, 0.5 C, 1 C and open end cycling at 0.1 C). Reprinted with permission from Ref. [54], Copyright (2017) American Chemical Society.

carbon-free composite cathodes. Here, the fraction of electrical inactive NCM increases with increasing particle size from 2% for the finest to 31% for the coarsest material tested, respectively.[58] To minimize contact losses during cycling stack pressure is applied.[19,59] Apart from this, the contraction of the active material can lead to micro cracks within the secondary particles of polycrystalline NCM active material enhancing capacity fading. The phenomenon increases with nickel content, temperature and applied voltage.[57,60,61]

2.3. Electrolyte-electrode-interphase

The cell performance of conventional LIBs with liquid electrolyte can be affected unfavorably by diffusion of parasitic side products and induce a "cross talk".[12] However, in SSBs the decay products remain on the electrolyte/electrode interface and form a resistant interphase. On the anode side, there are three distinctions for the contact between lithium metal and SE according to Wenzel et al.:[62,63] A non-reactive and thermodynamically stable interface, a reactive and conducting interphase, as well as a reactive and metastable interphase. The ideal interphase is a thin passivation layer of nanometers thickness which serves as ionic conductor, as well as electronic isolator. This way, the chemical potential of the lithium metal is reduced to the electrochemical window of the electrolyte.[64] In dependence to the applied voltage different phase equilibria can be obtained. For example, for Li_3PS_4 electrolyte with metallic Li the phase equilibria are Li_2S and Li_xP_x at low voltages, as well as P_2S_5 and S at high voltages, respectively.[64,65] On the cathode side, one study reports a significant growth of a cathode-electrolyte-interphase already during the first charging cycle within a Li-In I β-Li_3PS_4 I NCM 811 + Li_3PS_4 battery cell. The interphase is formed by an oxidation of the sulfidic electrolyte.[54] Especially for charging voltages above 4.3 V vs. Li/Li^+, a significant increase of interphase formation due to SE degradation was determined.[66] Moreover, depth profiling reveals that most degradation takes place near the current collector. This could be prevented by an appropriate passivation of the current collector.[66] To minimize interfacial resistance and also to improve contact between current collector, electrolyte, active material and anode stack pressure has to be applied during cycling of sulfidic SSBs.[67,68] There are several review papers which cover the electrode-electrolyte challenges in more detail.[64,69–71]

2.4. Large scale production

A further challenge is the large-scale production of SSBs at costs comparable to conventional LIBs. Here, it is important to provide cheaper electrolyte material, as well as reducing the reactivity of the sulfidic material.[1] Currently, most research on sulfide SSBs is based on lab-scale production. Basic understanding on interface characteristics and electrolyte degradation during cycling, for example, is often generated by pellet-type cells.[46,51,54,66,72,73] First approaches with respect to slurry-based processing like binder or solvent evaluations are reported.[59,74,75] Because laboratory production can only give indications for possible improvements,[76] continuous processing procedures like an extrusion-based slurry preparation or densification by calendering have to be established as further scaling steps. To achieve a low porosity and high ionic conductivity high pressures are needed for the densification of sulfidic cathodes or separators. One study reports a densification by a warm isostatic press (WIP) at 490 MPa of pouch cells using Li_6PS_5Cl as sulfidic electrolyte.[11] For Li_6PS_5Cl pellets fabrication pressures of 50 up to 1000 MPa for cold pressing are described.[19,77] In relation to calendering, it could be difficult to achieve such high compression, i.e., line loads. This underlines the importance to clarify the effect of other densification parameters like process temperature. First studies report processing in a dry room instead of glovebox systems, which is highly relevant for industrial production.[11,46] Apart from this, appropriate design and recycling principles have to be developed to minimize resource consumptions, the amount of toxic waste and emissions by solvents into the environment in order to establish sustainable concepts throughout the battery processing.[78–80]

3. Processing at Laboratory Scale

Figure 3 shows the process chain for manufacturing sulfidic SSBs as already established in a large number of laboratories. In addition to the cell fabrication from dry mixing to cell construction, the mechanochemical synthesis of the SE is shown in advance. The reason for this is the limited commercial availability of the material and the frequently resulting need to self-synthesize it. It includes the milling and grinding of the reactants in a planetary ball mill and the subsequent heat treatment of the powder in a furnace. In the case of cathode processing, this is followed by dry mixing of the SE with other powder components such as active material and conductive additive using a mortar and pestle. The powder mixture (or just the SE powder for separators) is now dispersed into a binder solution consisting of solvent and polymer binder, for which planetary ball mills, dissolvers or simple magnetic stirrers are used. The suspension is then applied to a carrier substrate by film applicators using the doctor blade technique. The solvent is evaporated directly on the coating equipment or in a (vacuum) oven. Besides this mixing and coating technique, there are also powder-based approaches, such as aerosol deposition[81] or dry coating processes.[82] However, because of the suspension-based focus of this publication, those are not considered in the following. SSB coin and pouch cells are constructed by cutting out samples from the layers and compacted using laboratory or isostatic presses. Finally, the construction of battery cells takes place.

3.1. Synthesis

Wu et al. stated three different methods which are usually used for synthesis of sulfide based SEs and explained them in detail: solid-state reaction (a), liquid phase (b) and a mechano-chemical ball milling method (c).[83,84]

a) In the solid-state reaction method, the reactants are first melted and then quenched or slowly cooled. This process usually takes place in quartz ampoules at temperatures of up to 1000 °C, which makes the process comparatively complex and poses problems regarding scalability. A number of highly conductive Li_2S-P_2S_5, Li_6PS_5Cl and $Li_{10}GeP_2S_{12}$ SEs were synthesized using this method. Influencing parameters are the reaction atmosphere, temperature and time, as well as the cooling rate.[25,83,85,86]
b) Liquid phase synthesis is carried out using the reactants of the SE and a suitable solvent, such as 1.2-dimethoxyethane, acetonitrile or tetrahydrofuran, followed by solvent evaporation. Despite lower ionic conductivities, possibly due to impurities of the solvent remaining in the SE after drying, lower interfacial resistances in the case of a SE-cathode application and good scalability of the process makes this technique interesting. Besides process time, energy input and temperature, relevant parameters are type and content of solvent, as well as possible additives and the drying settings. For example, $Li_7P_3S_{11}$, Li_6PS_5Cl and Li_6PS_5Br have been produced using this method.[83,87–89]
c) When synthesizing using a (planetary) ball mill, the reactants are ground and mixed at room temperature. This method is of high interest especially for amorphous SE manufacturing, e.g., Li_3PS_4. Partial crystallization can be achieved by high rotational speeds and consequently high temperatures or by subsequent temperature treatment, so the production of halide argyrodites with sufficient ionic conductivity is also possible. Parameters of interest are the operating parameters of the mill (speed and grinding time), the characteristics of the grinding media (density, degree of filling/amount of milling balls, and diameter), and the grinding chamber (material and volume). Also, the properties of the grinding material (degree of filling of the grinding media, cohesive properties, initial particle size etc.) have an effect.[34,83,90]

Overall, the mechano-chemical synthesis presents a good compromise between scalability and ionic conductivities: The combination of different processes (mixing, grinding, synthesis), as well as the availability of continuously operating aggregates (stirred ball mill, circular tube furnace if necessary) is more complex compared to liquid phase synthesis, but easier to transfer to industrial scale than the extremely high temperatures of the solid-state reaction method. In parallel, the ionic conductivities do not reach (independent of the material system) the level of the SEs obtained with the solid-state reaction method, but exceed those of the products of liquid-phase synthesis. For this reason, this process is examined in more detail below.

According to Table 2, a variety of SEs of the different classes mentioned in Table 1 have been produced using planetary ball mills (except $Li_{10}GeP_2S_{12}$, where a planetary centrifugal mixer (PCM) has been used) and optional heat treatment steps. The starting materials were fed in stoichiometric ratios and contained

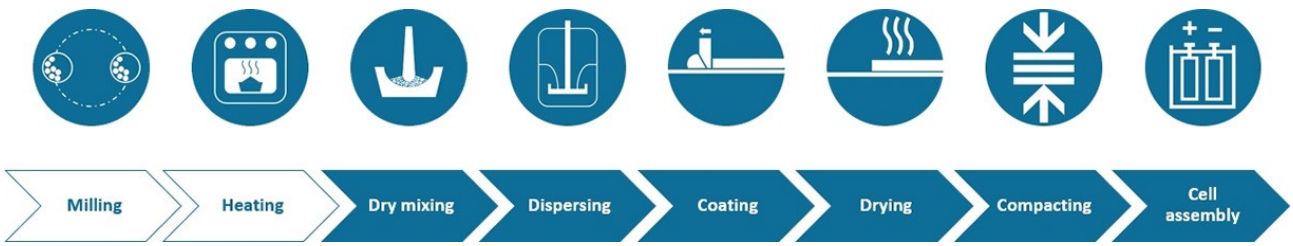

Figure 3. Process chain for the production of sulfidic SSBs on a laboratory scale from dry mixing to cell construction plus mechanochemical SE synthesis

Table 2. Mixing educts and heat treatments of sulfidic electrolytes by ball milling (*usage of a PCM instead of a planetary ball mill).

Material				Milling balls			Milling room			Process parameters		Heat treatment		Other	
Product	Reactant 1	Reactant 2	Reactant 3	Material [–]	Diameter [mm]	Quantity [–]	Material [–]	Volume [ml]	Speed [min^{-1}]	Duration [h]	Temperature [°C]	Duration [h]	Conductivity [$mS\,cm^{-1}$]	References
$60Li_2S$-$40Si_2S$	Li_2S	SiS_2	–	?	10	10	Al_2O_3	45	370	?	–	–	0.15	[33]
$78Li_2S$-$22P_2S_5$	Li_2S	P_2S_5	–	?	10	12	?	100	520	25	230	3	0.45	[36]
$78Li_2S$-$22P_2S_5$	Li_2S	P_2S_5	–	?	10	12	?	100	520	25	160/230	0.5/3	0.85	[36]
$80Li_2S$-$20P_2S_5$	Li_2S	P_2S_5	–	?	?	?	?	?	510	24	210	4	?	[7]
$Li_{10}GeP_2S_{12}$*	Li_2S	P_2S_5	GeS_2	ZrO_2	5	8	Plastic	12	2000	0.5	550	10	6.30	[24]
Li_3PS_4	Li_2S	P_2S_5	–	Al_2O_3	10	10	Al_2O_3	45	370	20	–	–	0.20	[34]
Li_3PS_4	Li_2S	P_2S_5	–	ZrO_2	2	42030	ZrO_2	500	250	20	–	–	0.40	[35]
Li_3PS_4	Li_2S	P_2S_5	–	ZrO_2	5	309	ZrO_2	80	500	10	243	1	1.00	[24]
Li_6PS_5Br	Li_2S	P_2S_5	LiBr	ZrO_2	10	15	ZrO_2	45	600	10	550	5	0.62	[26]
Li_6PS_5Cl	Li_2S	P_2S_5	LiCl	ZrO_2	10	15	ZrO_2	45	600	20	550	5	1.33	[26]
Li_6PS_5I	Li_2S	P_2S_5	LiI	ZrO_2	10	15	ZrO_2	45	600	20	550	5	0.19	[26]
$Li_7P_3S_{11}$	Li_2S	P_2S_5	–	Al_2O_3	?	?	Al_2O_3	?	500	40	300	2	3.20	[22]

Li_2S and (with one exception) P_2S_5. A third reactant each was added for $Li_{10}GeP_2S_{12}$ and the halide argyrodites.

The influence of the mechanochemical milling on the synthesis of solid electrolytes can be split into three categories: The properties of the grinding media (density, diameter and number) and grinding chamber (material, volume) used as well as the operating parameters (speed, duration) of the mill. A comprehensive description has been given by Schlem, Burmeister et al. and can be used as a basis for the selection of suitable grinding media properties.[90] In summary, they state that the mechanochemical milling provide sufficient stress energies to induce particle breakage, the mixing of educts, as well as the energy for chemical conversion. Given from their point, as well as from the literature, stated here, it is difficult to make a general statement about optimum process conditions.

In the syntheses investigated, grinding media made of Al_2O_3 or ZrO_2 were used, but in one third the specification is missing. Although both materials are electrically insulating and therefore do not negative effect the product in case of abrasion (e.g., short-circuiting of a cell due to contamination of the SE in the separator by preceding steel abrasion), the density of ZrO_2 (5.68 g/cm^3) is higher in comparison to Al_2O_3 (3.94 g/cm^3), which increases the stress energy at constant grinding media diameter. For this reason, the use of ZrO_2 is expected to be favorable. The diameters range from 2 to 10 mm even for the same product, thus no systematic approach can be identified. Due to the larger specific surface area of smaller grinding media and the resulting worse yield caused by adhesion of the product to the milling beads, larger grinding media are preferred. The number of grinding balls varies between 8 and 42,030, in addition to the choice of grinding media diameter, this depends partly on the different grinding chamber volume in the literature listed and does not necessarily allow a statement about the process conditions. The grinding chamber properties are characterized by the material of the inner wall lining and the volume, from which the grinding media and regrind filling degree are derived. The grinding chambers of planetary ball mills are lined with Al_2O_3 and ZrO_2, the only exception is the PCM with a plastic process chamber. According to the insulating properties of the materials, all of them can be used; to avoid abrasion, Al_2O_3 and ZrO_2 are preferable. Due to many unknowns and variables with regard to bulk densities, grinding material and grinding media quantities, as well as reactants used, no comparative statement can be made on the powder filling ratios. Hence, the above-mentioned specifications by Schlem, Burmeister et al. can be referred to and some basic guidelines in terms of process design can be followed:[90]

The grinding media filling ratio should be between 0.3 und 0.5, as a compromise between power input, stress frequency and stress energy, as the highest stress energies are reached at low fillings, while in regard to highest power and higher frequencies, medium ratios are favorable. The powder filling ratio is analogously selected between 0.5 und 1. Rather than from the filling ratio, the stress energy shall be controlled via the grinding media diameter and speed: larger media lead to higher stressing energies, but also reduce the number of media at constant filling. And, for small beaker volumes (45 mL) as

presented here, the larger media can be less favorable due to hindered motion. The change in media size at constant filling often does not change the power input, but by the speed the energy of stressing as well as the power can be increased, leading to reduced duration and better conductivity.

If only the electrolytes synthesized in planetary ball mills are considered, the rotational speeds range between 250 and 600 rpm, while the process lasts between 10 and 60 h. The PCM once again falls out of line with 2000 rpm and 0.5 h process time. However, the mills P7 and P5 mills (Fritsch GmbH), which were mainly used to conduct the experiments in this review, can be operated even at larger speeds, and thus leave the possibility for further optimization. A closer view on the processing of Li_3PS_4 shows the advantage of larger stress energies due to larger media densities, larger media or higher speeds, so that is recommended to choose parameters in regard to high stress energies to obtain higher conductivities. An improvement of conductivity is also possible through longer residence times.[26,90] However, while high rotational speeds are recommended, the residence time can be kept to the necessary minimum by regularly checking the comminution progress, thus making the process more energy efficient.

If a XRD measurement shows only partial crystallization of the SE after the grinding process, this can be supplemented by heat treatment. The temperatures range between 160 and 550 °C, the duration is between 0.5 and 10 h. Comparable values are only available for the synthesis of $78Li_2S–22P_2S_5$, but show almost a doubling of the ionic conductivity,[36] by extending the heating duration for 0.5 h at only 160 °C therefore subsequent heat treatment is highly recommended.

Despite the high number of possible process optimizations, the lack of literature data on this suggests a neglect in the establishment of the synthesis process. Consideration of comprehensive process engineering studies on the energy-efficient synthesis of SEs is recommended.

3.2. Formulation

3.2.1. Cathodes

Cathodes for sulfidic SSBs usually consist of the active material, the electrolyte, a binder, as well as a conductive additive (see Figure 1).[12] As the main compound in weight, active materials like olivines (e.g., $LiFePO_4$), layered oxides (e.g., $LiNi_xCo_yMn_zO_2$) or spinels (e.g., $LiMn_2O_4$) are used in general.[57,78] In literature, usually mass fractions of 60% to 81% are described (see Table 3), although only mass fractions of more than 70% are economically interesting.[91] NCM-based materials are considered as one of the most promising candidates for SSBs.[92] In contrast to fully commercialized NCM 622, NCM with higher nickel content has to be evaluated for cathode processing to enhance energy density and reduce material costs.[57,93] However, in comparison to LIBs with liquid electrolyte SSBs with nickel-rich NCM materials show lower initial reversible capacity. This may be due to interfacial characteristics, lower ionic conductivity, as well as chemo-mechanical processes.[93] To minimize unintentional

Table 3. Cathode layer formulations with different types and amounts of active material, SE, conductive additive and binder *coated with $LiNbO_3$, **LZO (formulations are normalized to 100 wt%).

Cathode active material		Electrolyte		Conductive additive		Binder		Electrochemical performance		References
Mass fraction [wt%]	Type [–]	Mass fraction [wt%]	Type [–]	Mass fraction [wt%]	Type [–]	Mass fraction [wt%]	Type [–]	1st Discharge capacity [mAh/g_{NCM}]	Test parameters	
66.0	NCM* 111	28.3	LPS	2.8	AB	2.8	SEBS	158	0.04 C, 30 °C	[35]
66.0	NCM* 111	28.3	LPS	2.8	AB	2.8	SBS	121	0.04 C, 30 °C	[35]
81.3	NCM** 955	14.4	LPSCl	2.9	CNF	1.4	PTFE	215	0.2 C, 60 °C	[11]
68.1	NCM* 622	29.2	LPSCl	1.3	C65	1.4	NBR	133	0.1 C, 30 °C	[111]
78.1	NCM* 622	19.2	LPSCl	1.3	C65	1.4	NBR	122	0.1 C, 30 °C	[111]
83.1	NCM* 622	14.2	LPSCl	1.3	C65	1.4	NBR	95	0.1 C, 30 °C	[111]
60.0	NCM 811	35.0	LPS	2.0	DB	3.0	NBR	138	0.1 C, ?	[16]
67.2	NCM 622	28.8	LPS	2.0	C65	2.0	PIB	110	0.05 C, 60 °C	[112]
67.2	NCM 622	28.8	LPS	2.0	VGCF	2.0	PIB	140	0.05 C, 60 °C	[112]
69.0	NCM 85I05I10	29.0	LPS	–	–	2.0	PIB	150	0.1 C, 25 °C	[113]
67.0	NCM 85I05I10	31.0	LPSI	–	–	2.0	PIB	178	0.1 C, 25 °C	[113]
71.2	NCM* 622	23.7	LPS	2.0	S65	3.0	HNBR	152	0.2 C, 20 °C	[59]

reactions with the electrolyte and to achieve favorable interface characteristics, protective coatings have to be identified.[92,94] To reduce the interfacial resistance $LiNbO_3$ is commonly used as coating material, but further optimization has to be done due to the brittle character of $LiNbO_3$.[92,95–97] Another important property of the active material is the particle size distribution and the resulting contact area between the active material and electrolyte. Small active material particles increase the electrical conductivity in carbon-free ASSBs due to a higher surface area and an increased formation of percolating electronic clusters.[58,98–100] Also, smaller particles deliver short lithium ion diffusion paths within the active material but also increase electrolyte degradation due to a higher surface area.[98,99] Shi et al. report the achievement of higher energy dense pellet-type cathodes by reducing the particle size of the electrolyte ($75Li_2S–25P_2S_5$) from an average size of 8 μm, 5 μm, 3 μm to 1.5 μm and increasing the average active materials particle size ($Li_2O–ZrO_2$-coated $LiNi_{0.5}Co_{0.2}Mn_{0.3}O_2$) from 5 μm to 12 μm.[100] They also used carbon nanofibers (CNF) as conductive carbon additive. Another study compared the electrochemical performance in pellet-type cells of a composite cathode with a fine (x_{50} = 2.6 μm), a coarse (x_{50} = 14.1 μm), as well as a mixture of both different sized $78Li_2S–22P_2S_5$ glass ceramic electrolytes.[101] NCM 622 with an average size of 6.9 μm was used as active material and Super-P carbon as conductive additive. The best electrochemical performance was obtained for a weight ratio of 1 : 3 of the coarse to fine electrolyte material. This result could be attributed to a larger contact area between electrolyte and active material, as well as a denser electrode structure.[101] However, a complete embedding of the active material within the electrolyte seems to have a detrimental effect on the electrical conductivity of the cathode, at least when no conductive additive is used, due to an electrical isolation of the particles.[102]

These results demonstrate the importance of the particle sizes of the active material in relation to the electrolyte and has to be evaluated carefully for the individual material type used. Furthermore, the impact of the crystalline state (single- or polycrystalline) of the layered oxides has to be investigated in more detail.[103] One aspect may be the fact that the SE cannot fill the pores of the primary particles within the polycrystalline active material. Moreover, high pressures during compaction can cause a breakage of the polycrystalline material.[93,104] As mentioned before, the higher surface of the single crystalline material can result in a higher degradation because of the larger contact area to the electrolyte. Also, the particle size can affect the viscosity behavior of the electrode slurry and thus, the needed amount of solvent.

The second main compound in weight within the cathode is the SE (see Table 3). Potential sulfide-based electrolytes and their theoretical ionic conductivity are described in detail in the Introduction and listed in Table 1.

Conductive additives are employed to achieve a homogeneous current distribution, high power density, as well as to avoid overcharging.[105] They can improve electrical conductivity of the electrode.[106] In this context, an improved battery performance can probably be achieved by using VGCF (diameter: 100 nm, length: 20–200 μm)[52] or carbon nanofibers instead of commonly used carbon black.[107,108] Nevertheless, strict safety measures will be inevitable due to their high aspect ratio and carcinogenic impact,[109] complicating dry mixing steps to prestructure the composites. Handling the carbon fiber powder within suspension is one possibility to lower safety risks but could complicate scaling up of the battery cell production. Furthermore, conductive additives can induce a decomposition of the electrolyte resulting in an increase of the interfacial resistance and a stronger capacity fading.[52,105] One study reports a larger interfacial charge-transfer resistance within a composite pellet-type cathode with $Li_{10}GeP_2S_{12}$ due to the incorporation of carbon. Whereas the carbon-free solid state battery reached a first discharge capacity of 123 mAh g^{-1} at 0.1 C, batteries with Denkablack, Super PLi, Graphite, Ketjenblack and Super C65 only reached 94 mAh g^{-1}, 112 mAh g^{-1}, 92 mAh g^{-1}, 90 mAh g^{-1} and 103 mAh g^{-1}, respectively.[105] Another study reports a better initial discharge capacity between 144 and 155 mAh g^{-1} for $Li|\beta\text{-}Li_3PS_4|LiNi_{0.6}Co_{0.2}Mn_{0.2}/\beta\text{-}Li_3PS_4$ pellet-type cells with VGCF at 0.1 C and 25 °C proberbly due to an advantageous electrical percolation network and redox-active decomposition products of the SE. Cells without VGCF achieved only 98 to 128 mAh g^{-1}. However, the VGCF induced a significant capacity fading during cycling, which falls below the performance of the cell without VGCF after 62 cycles.[52]

For carbon-free SSBs, only active materials with sufficient electrical conductivity like $LiCoO_2$ are practicable.[105,110] Furthermore, a transfer to slurry-based electrodes has to be evaluated carefully. The binder as electrochemical inactive compound further decreases the electrical conductivity. Moreover, conductive additives are probably necessary to achieve good performance at high C-rates.[106]

The binder is necessary for a good adhesion between the active material, electrolyte and, if used, conductive additive, as well as for sufficient cohesion to the current collector. To roll up the cathode and separator which is advantageous for continuous production an excellent mechanical stability to avoid any flaking off is needed. To obtain a higher energy density the binder content should be kept low and has to be evaluated carefully.[59,75] In Table 3 some examples of binders used for sulfidic SSBs are listed.

3.2.2. Separator

Slurry-based separators consist of a binder and SE. Formulations found in literature for sulfidic SSBs are described in Table 4. Usually, the content of electrolyte varies between 90 wt% and 99 wt%. As for the cathodes, the binder content should be kept to a minimum to ensure a dense electrolyte structure. Probably, the solids content to achieve a coatable suspension is mainly dependent on the electrolyte properties like particle size and less on the binder used (compare Table 4). Also, the particle size distribution of the electrolyte can affect the solvent evaporation during drying (see Section 3.3.2. wet coating and drying).

Table 4. Separator formulations with different types and amounts of SE and binder (formulations are normalized to 100 wt%).

Electrolyte		Binder		Electrochemical performance		References
Mass fraction [wt%]	Type [–]	Mass fraction [wt%]	Type [–]	Conductivity [mS cm^{-1}]	Densification state and temperature	
97.0	LPS	3.0	SBS	0.2	25 °C, 410 MPa	[35]
97.5	LSPS	2.5	PIB	2.4	30 °C, calendered	[74]
90.0	LSPS	10.0	PIB	2.2	30 °C, calendered	[74]
97.5	LSPS	2.5	SBR	1.6	30 °C, calendered	[74]
90.0	LSPS	10.0	SBR	1.8	30 °C, calendered	[74]
97.5	LSPS	2.5	PEVA	3.2	30 °C, calendered	[74]
90.0	LSPS	10.0	PEVA	1.5	30 °C, calendered	[74]
97.5	LSPS	2.5	HNBR	3.2	30 °C, calendered	[74]
90.0	LSPS	10.0	HNBR	2.3	30 °C, calendered	[74]
99.0	LPSCl	1.0	AC	1.3	RT, 300 MPa	[11]
96.0	LPS	4.0	NBR	0.4	?	[16]
98.0	LPS	2.0	PIB	?	–	[112]
97.0	LPS	3.0	HNBR	0.1	400 MPa, 20 °C	[59]

3.2.3. Anodes

Lithium metal as anode could provide the highest theoretical capacity with 3860 mAh g^{-1} and lowest standard electrochemical potential with −3.04 V vs. the standard hydrogen electrode.[114,115] However, lithium-metal has the tendency to form dendrites.[114,116,117] Dendrites increase the risk of thermal runaway and explosion caused by short circuit.[114] Because of the high mechanical stability of SEs and resultant prevention of dendrite formation the use of lithium metal anodes may be possible.[12] Despite first assumptions most SEs are thermodynamically instable against lithium at high and low potentials.[116] However, due to the formation of a passivation layer by decomposition reactions the electrolyte is kinetically stabilized against lithium, which can also be improved by appropriate interface engineering.[116] Some sulfidic electrolytes like $Li_{9.54}Si_{1.74}P_{1.44}$ $S_{11.7}Cl_{0.3}$ and $Li_{9.6}P_3S_{12}$ seem to have a high ionic conductivity and electrochemical stability versus lithium metal.[118] To avoid any side reactions between the electrolyte and anode, indium foil is often used as anode on the lab scale.[54,59,66,119] However, due to its high costs and low energy density it is economically not feasible.[91] Also, the use of composite anodes including the SE is described with graphite, silicon or a silver nanoparticle/carbon black mixture as active material (see Table 5). This way, already pouch cells have been built successfully.[11,111] Due to the larger surface area provided by the composites, higher current densities can be achieved with still homogeneous Li-deposition. However, graphite anodes can be used for first investigations but cannot enhance the energy density of the battery in comparison to conventional LIBs. The uncontrollable dendrite growth in case of a lithium metal anode is caused by the locally competing SEI formation and charge storage. In contrast, the SEI formation and charge storage for anode materials, which allows the intercalation of lithium ions, is locally separated and therefore controllable.[120] Moreover, one study reports a battery cell with Li_6PS_5Cl as electrolyte and a columnar silicon anode with a practical capacity of 3.5 mAh cm^{-2}.[121]

3.3. Electrode and separator processing

3.3.1. Dispersing

3.3.1.1. Dry mixing

For a first deagglomeration of the conductive additive and a homogenization of the individual powders used in the compo-

Table 5. Anode layer formulations with different types and amounts of active material, SE, conductive additive and binder (formulations are normalized to 100 wt%).

Anode active material		Electrolyte		Conductive additive		Binder		Electrochemical performance	References
Mass fraction [wt%]	Type [–]	Mass fraction [wt%]	Type [–]	Mass fraction [wt%]	Type [–]	Mass fraction [wt%]	Type [–]	1st Discharge capacity [mAh/g_{NCM}]	
55.8	GP	40.4	LPS	1.0	AB	2.9	SBS	322	[35]
23.4	AG	–	–	–	–	7.0	PVDF	?	[11]
69.8	CB								
58.6	GP	39.1	LPSCl	–	–	2.3	NBR	330	[111]

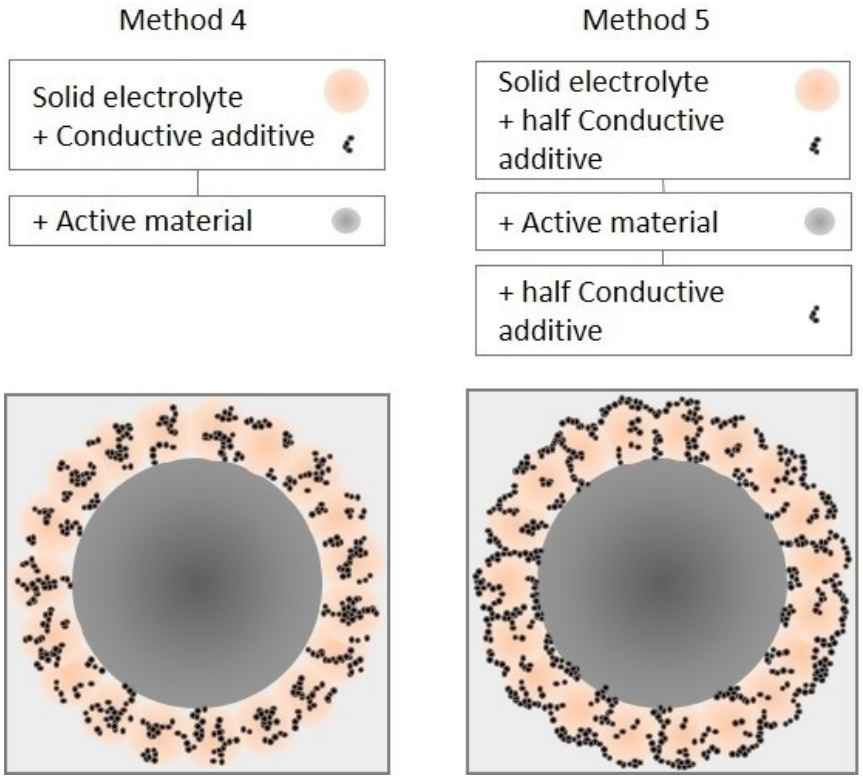

Figure 4. Mixing protocols and anticipated microstructures for sulfidic SSBs. Adapted by permission from Springer Nature Customer Service Center GmbH from Ref. [72]: Springer Nature, Copyright 2018.

site cathode or anode (active material, electrolyte and conductive additive) dry mixing can be performed before wet dispersing.[78] The binder is usually solved in the solvent before,[59] but in dependency which binder type is used, it can probably also be mixed dryly with the other compounds.[78] In contrast to conventional electrodes, composite cathodes and anodes for SSBs contain the electrolyte as one further dry compound probably affecting the agglomeration behavior of the conductive additive or active material significantly. Sometimes a first grinding by mortar and pestle before wet dispersing is described for this purpose.[74,112,113] One study also reports a pre-mixing of NCM 622 and Li_6PS_5Cl by mechanical milling. They describe a first-cycle discharge capacity of 127 mAh g^{-1} of half-cells at 0.1 C and 30 °C in comparison to 95 mAh g^{-1} for a not premixed formulation indicating a more favorable ionic conductivity.[111] Another study[72] tested five different dry mixing protocols for pellet-type cells with mortar and pestle, which are often used for a component homogenization before pelletizing the powders.[7,54,66,103] Methods 4 and 5 (see Figure 4) showed the best electrochemical performance with a first cycle discharge capacity of 150.5 mAh g^{-1} and 144.0 mAh g^{-1} at 0.05 C and room temperature respectively. At 1 C the detected discharge capacity was 32.4 mAh g^{-1} (method 4) and 54.2 mAh g^{-1} (method 5).[72] Presumably, due to the first pre-mixing of the conductive additive and electrolyte, the conductive additive concentrated upon the electrolyte surface. The addition of a portion of the conductive additive at the end causes advantageous electron pathways within the interspaces of active material particles (method 5).[72] This study demonstrates the significance of powder mixing on the resulting electrode microstructure for pellet-type cathodes and can give important hints for an effective pre-mixing before wet dispersing. However, because mixing by hand with mortar and pestle are non-reproducible due to an uncontrollable force input and user dependency as well as it is not scalable automated methods have to be established (see Scale-up). Furthermore, while first results in terms of pre-mixing are obtained for sulfide-based composite cathodes, the importance for composite anodes also has to be investigated.

3.3.1.2. Wet dispersing

Particularly important in the process chain for the production of sulfide based SSBs is the wet dispersion process. Besides transferring the powder raw materials and solvent into a coatable, homogeneous suspension, the SE and conductive additive particles are dispersed, which is necessary to form the percolation networks for electrical and ionic conduction within the electrode. A suitable viscosity for the subsequent coating is set. For this reason, the aggregates and process parameters used by the different research works are compared in Table 6.

Mostly, a PCM by Thinky U.S.A Inc. is used for wet dispersion (sometimes supported by milling balls[11] or extrend by ultrasonic homogenizing[97]). Their largest mixer can process a product quantity of 14.5 kg. The motion pattern is similar to the grinding

Table 6. Wet processing of cathodes, separators and anodes with different aggregates, parameters and solvents.

Aggregate/method	Components	Speed [min^{-1}]	Time [min]	Solids content [wt%]	Solvent [–]	References
Dissolver	Cathode	2870	60	40	p-xylene	[59]
Dissolver	Separator	2870	60	30	p-xylene	[59]
Mortar/ Pestle	Cathode	–	–	40	p-xylene	[113]
Mortar/ Pestle	Cathode	–	–	60	p-xylene	[113]
Aggregate/method	Components	Speed [min^{-1}]	Time [min]	Solids content [wt%]	Solvent [–]	References
Mortar/pestle	Cathode	–	–	?	p-xylene	[16]
Mortar/pestle	Cathode	–	–	25–27	Toluene	[112]
Mortar/ pestle	Separator	–	–	50	p-xylene	[113]
Mortar/pestle	Separator	–	–	14–16	Toluene	[112]
PCM	Anode	?	?	?	NMP	[11]
PCM	Anode	?	?	?	Anisole	[35]
PCM	Cathode	?	?	65	Heptane	[35]
PCM	Cathode	?	?	65	Anisole	[35]
PCM	Separator	?	?	65	Anisole	[35]
PCM + ZrO_2 balls	Separator	2000	6	?	Xylene IBIB (1/1)	[11]
PCM + Ultrasonic	Cathode	1600	31	?	n-decane	[97]
PCM + Ultrasonic	Cathode	1600	31	?	Toluene	[97]
PCM + Ultrasonic	Cathode	1600	31	?	1,2-dichloroethane	[97]
Stirring	Separator	?	>720	20–45	Toluene	[74]

chamber in a planetary ball mill, with a chamber tilted at a 45° angle and rotating around a center point and itself in opposite direction (Figure 5a). The inclination of the chamber is intended to guarantee a three-dimensional flow of material. According to the manufacturer a turbulent flow profile involves strong shear forces and enables the production of homogeneous suspensions despite high viscosities.[122]

In comparison, dissolvers with product volumes of up to 2,000 l are available. The use of a rotating toothed disc leads to a formation of a drum and a characteristic, donut-shaped flow profile (Figure 5b). Agglomerates are stressed and dispersed by the collision with the dispersing tool, but mainly by the turbulent flow. Degassing by applying vacuum, as well as tempering of the process by a heating and cooling jacket are possible.[123] For high viscous suspension usually planetary mixers are employed instead of a dissolver. Besides the fast rotating toothed disc, they are equipped with a slowly rotating stirrer and a rotating wall scraper to ensure the motion of the entire vessel content.[124] For even higher solids content, kneaders can be used.[125]

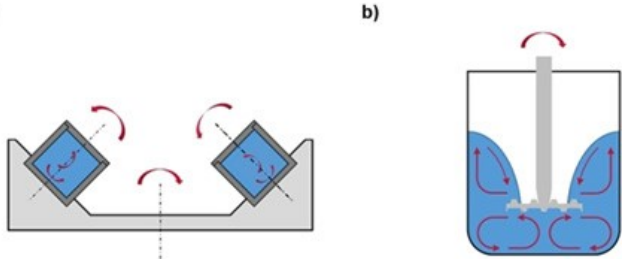

Figure 5. Schematic illustration of the a) PCM b) dissolver, as well as its flow profile.

Furthermore, in a small lab scale, dispersion is carried out with the aid of mortar and pestle or using magnetic stirrers. These methods are only recommended to a limited extent, as they are partly user-dependent, constant stress profiles with high shear intensities do not develop and the adjustment of defined process parameters is not possible. Otherwise, different speeds and dispersion times are applied depending on the dispersing machine (1,600–2,000 rpm and 3–6 min at the PCM, 2,870 rpm and 60 min at the dissolver). Although systematic process parameter variation for rotational speed and residence time on dissolvers and extruders has only been performed in the production of conventional LIBs,[126,127] a difference in shear intensity can be stated based on indications from the work of Teo et al. for PCM based production[128] and by Batzer et al. for dissolver based preparation.[59] In both research works PIB is used as a binder but divergent results with respect to the adhesion strength of the coatings were achieved. While stable coatings can be produced after mixing in a PCM even with lower binder contents, the coatings whose suspension has been processed using a dissolver are brittle and fragile. Assuming a constant viscosity, this could be explained by a more shear intensive dispersion process in the dissolver. Here, the binder network could negatively impacted, however, agglomerates of the conductive additive are broken up even better. However, this assumption must be put into context with the different process and analysis parameters. The selected solvents and the solids content of the suspensions are closely related to the previous Section 3.2. Formulation, as well as to the subsequent coating step. Because the binder is added to the solvent in

general before the powder is dispersed in it, a suitable solubility in the solvent is needed. Furthermore, all other materials, especially the sensitive sulfidic SE, must be stable in the solvent. After conducting extensive solvent studies, p-xylene, toluene, heptane and anisole are often used.[16,35] The solids content, as well as size and therefore specific surface of the particles are mainly responsible for the viscosity of the suspension. It must be chosen low enough to allow coating, e.g., using the doctor blade technique, and at the same time as high as possible to avoid the evaporation of large amounts of solvent and consequently the segregation of the particulate components in the electrode layer.[129]

3.3.2. Wet coating and drying

For suspension coating, only film applicators and the doctor blade technique are used (based on publications listed in Table 7, only[11] manufactured their anode with a screen printer). The coating speed of the doctor blade is only given by Batzer et al. with 0.3 m min^{-1}.[59] Further parameters are given in Table 7. The reported gap widths vary between 200 and 500 µm. For anodes and cathodes, the carrier substrate is the current collector (copper or stainless steel (SUS) for anodes, aluminum for cathodes), possibly including a carbon coating for better electrical contact. Separators, on the other hand, are either processed on release foils (PE, PTFE) for later free-standing deposition on cathode or anode layers, or are coated directly on the electrodes for lower interfacial resistances.

The drying behavior of cathodes and separators is strongly affected by the used particle size. Figure 6 demonstrates the solvent evaporation in dependence to the particle size of the electrolyte in separator layers. Layers consisting only of fine material may be prone to cracking during the drying process. The upper part of the separator layer dries much faster in comparison to the lower ones, because the dense structure impedes the solvent from evaporating (see Figure 6a). This effect also increases with increasing thickness of the layer. Using sulfide particles with a broader particle size distribution (see Figure 6b and c) result in a more consistent solvent evaporation and therefore, can prevent the formation of cracks. Delaying solvent evaporation by low temperatures and high vapor pressures above the film thus seems desirable. This is also reflected in the drying parameters selected for the first drying step directly on the plate of the film applicator: The temperatures for drying electrodes are usually between 70 and 80 °C. For separators, the drying temperature is usually between 20 and 25 °C; only once was drying carried out at 50 °C. The drying time for electrodes and separators varies greatly from a few minutes up to 20 h. For a second drying step a storage overnight in a vacuum oven is often described. The temperatures here reach up to 100 °C to dry out the last remaining solvent to avoid a reduction in ionic

Table 7. Coating and drying of cathodes and separators using film applicators and vacuum ovens.

Component	Gap width [µm]	Substrate	Temperature [°C]	Time Vacuum [h]	Temperature vacuum [°C]	Time [h]	References
Anode	–	SUS	80	20	100	12	[11]
Cathode	?	Aluminum	20	1	60	24	[16]
Cathode	300	Aluminum	–	–	20	Overnight	[112]
Cathode	300	Aluminum	70	1/4	–	–	[59]
Separator	?	Release	25	?	–	–	[35]
Separator	200–400	Release	20	1	?	12	[74]
Separator	?	Release (PTFE)	50	Few minutes	40	Overnight	[11]
Separator	?	Cathode	20	1	60	24	[16]
Separator	300	Cathode	–	–	20	Overnight	[112]
Separator	300	Release (PE)	–	–	20	Overnight	[112]
Separator	500	Cathode	20	Overnight	–	–	[59]

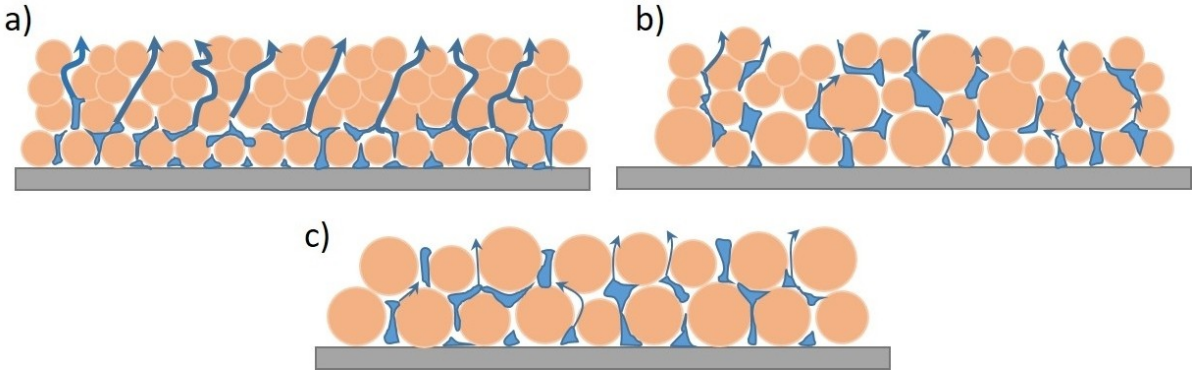

Figure 6. Drying behavior of the separator in dependence on the particle size of sulfidic electrolyte. Solvent evaporation is shown by blue arrows. The thinner the arrows, the more consistent is the evaporation. a) Small particle size: Impeded solvent evaporation in the lower layer of separator by small voids. This phenomenon promotes the formation of cracks within the layer. b) Mixture of fine and coarse particles. c) Coarse particle size form greater voids resulting in a more uniform solvent evaporation.

conductivity. Because of the small quantities involved, cracking may no longer be an issue. However, longer drying times are unfavorable from an economic point of view, making further development work necessary for scaling purposes.

3.3.3. Densification

Similar to the processing of LIBs, the densification step is of high importance to improve mechanical properties like adhesion strength, as well as to enhance the volumetric energy density and electrical and ionic conductivity. An important difference is the minimization of porosity in SSBs: As there is no liquid electrolyte to fill them later on, voids raise the tortuosity of the ionic pathways. While in conventional LIBs the ion transportation via the liquid phase and the electron transportation via the solid structure are two competitive processes,[130] in SSBs only the solid structure is relevant. The contact area between sulfidic electrolyte and active material can also be maximized by compacting and, thus, interface characteristics can be improved. In Figure 7, different possibilities to compress sulfidic separators and electrodes are illustrated. Probably, the simplest method in terms of handling and time requirement is to coat the separator directly onto one electrode and to compress them. The combined densification may also increase the adhesion strength between the components. On the other hand, the use of the same binder in the separator and electrode can result in a mutual dissolution at the interface,[46,74] while a free-standing separator can be advantageous.[74] Also, different densifications conditions with respect to temperature, pressure and line load may be beneficial for the electrodes and separator, respectively. This could be realized by a separate compression of the electrodes and separator.

Studies already confirm a higher ionic conductivity of pelletized sulfidic electrolyte with increasing densification pressure due to a reduction of voids.[19,73,131] In this context, Doux et al. report an increase of relative density of a pellet-type separator from 68.3 % to 75.4 % and of ionic conductivity from 0.99 mS cm^{-1} to 2.06 mS cm^{-1} when increasing the molding pressure from 50 to 250 MPa to Li_6PS_5Cl pellets.[19] However, stress distribution during the compaction of composite cathodes and probably also composite anodes is more complex. Ohashi et al. describe a non-uniform stress distribution within a composite cathode illustrated by zirconia replacing an active material and $Li_{10}GeP_2S_{12}$ as electrolyte. Here, stress is concentrated on materials with higher Young's modulus like NCM active material. The stress on softer sulfidic electrolyte is lower than the applied pressure and depends on the fraction of the material with higher Young's modulus.[132] Furthermore, they argue that due to a lower stress on the electrolyte the resistance is increased and a potential gradient is formed around the electrolyte region. Consequently, the ionic conductivity is reduced.[132] Besides, high pressure can cause a collapse of secondary NCM particles resulting in an increase of the charge transfer resistance and dead spaces within the material that are electrochemical isolated.[93] Another study reports a higher initial discharge capacity despite a higher internal resistance for slurry-based cathodes and separators fabricated at lower pressure. They first compacted the cathode (37 MPa) and afterwards the cathode-separator-combination with 74 to 111 MPa achieving 131 to 150 mAh g^{-1}, as well as 166 to 333 MPa achieving 108 to 125 mAh g^{-1}.This may be due to a fracturing of the polycrystalline NCM 111 and electrolyte used confirmed by FIB-SEM analysis.[97] Apart from this, high-pressure densification or calendering may also disturb mechanically weak networks of conductive additives within the electrode and therefore, deteriorate the electrochemical performance like it has been confirmed for conventional cathodes.[133] In order to realize a compaction, usually a densification of the composite cathode and separator is performed by a uniaxial press. This applies both to powder-based, as well as solvent-based cathodes and separators.[19,54,66,108] Another possibility is to compress entire pouch cells in a warm isostatic press like Lee et al. with a pressure of 490 MPa.[11] Here, a compression without wrinkling or loss of material due to flake off can be achieved.

Compacting parameters found in literature for sulfidic SSBs are listed in Table 8. Unfortunately, detailed information is often

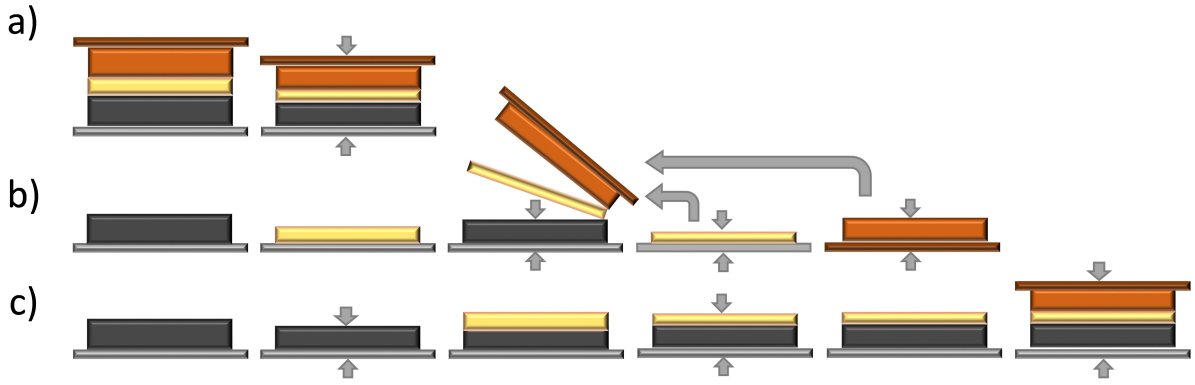

Figure 7. Different possibilities for densification as example: a) The separator (yellow) is coated directly on the cathode (black, current collector in grey), both are compressed together with the anode (orange, current collector in brown). The densification is demonstrated by arrows. b) Separator and electrodes are compressed individually. The separator is placed between the electrodes afterwards. c) The cathode is compressed. Next, the separator is coated onto the cathode and the composition is compressed together. Afterwards, cathode, separator and anode are compressed to one compartment.

Table 8. Compacting of cathodes and separators at different pressures and temperatures according to their porosity.

Component	Aggregate/ method	Pressure [MPa]	Temperature [°C]	Density (initial) [%]	Density (compacted) [%]	References
Cathode	?	330	25	?	?	[35]
Pouch cell	WIP	490	?	?	?	[11]
Separator	?	330	25	61	80	[35]
Separator	?	410	25	61	85	[35]
Separator	Calender	?	60	?	70-92	[74]
Separator	Uniaxial lab press	400	RT	?	?	[59]

not given illustrating the need for specific studies and higher attention on the densification process.

3.4. Cell assembly

Layer-based SSBs are based on punched or cut-out cathode, separator, and anode layers that are stacked to form a cell. Contacting and cell construction depend on the format of the cell: While circular samples can be put inside a Teflon tube, plugged on both sides with sealed metal stamps and these connected to the measuring instrument;[19,59,119,134] rectangular, large-format pouch cells are contacted with conducting tabs and sealed (see Figure 8).[11,111] Due to their simple and fast design, the first cells mentioned are recommended for extensive parameter variations and characterizations, while the latter are essential for practical application.

In Section 2 Challenges of sulfidic electrolytes, a low interfacial resistance between the different layers was highlighted as elementary for the function of an SSB. This is mostly ensured by applying a defined pressure during cyclization. For this reason, Doux et al. have investigated the dependence between operating pressure and ionic conductivity respectively cycling performance. They used powder based LPSCl separators, cathodes consisting of LPSCl and LNO-coated NCA, as well as Li–In as an anode. Impedance measurements on the separator showed an increase in ionic conductivity by an order of magnitude when a pressure of 70 MPa was applied and titanium current conductors were used. However, if carbon powder is used instead, the influence is smaller, the conductivity is improved only up to approximately 25 MPa. This is analogous to cycling and is explained by the better contacting of the soft SE.[19,59] Therefore, to apply a defined pressure, a wide range of cell press devices have been developed. Three of them are explained in the following.

Figure 8. Structure of different cell formats. a) Measuring cell consisting of two metal dies, a Teflon tube, as well as electrode and separator layers. b) Pouch cell consisting of press inserts, as well as electrode and separator layers (pouch foil not displayed).

The first cell press device (Figure 9a) consists of four screws and nuts each, two steel plates and isolators each and a measuring cell: After the measuring cell or the pouch cell are positioned between the insulated steel plates, pressure is applied centrally to the device with a uniaxial press. Next, the four screws at the corners of the device are tightened alternately until the indicated pressure of the uniaxial press drops and the force is carried by the screws of the cell press device. Alternatively, the screws can be tightened alternately using an external press or a torque wrench. In this case, the required torque is determined as a function of the sample area, the targeted pressure and a calibration line previously recorded using a load cell. Regardless of the method of applying the force, the disadvantage of this setup is the at least temporarily uneven distribution of force due to the successive tightening of the screws. In addition to the possibility of tilting, this affects the sample and cell performance. The advantage is the simple and low-cost design. A cell press device with multiple, separately bolted columns is used, for example, by Doux et al.[19,134]

The second cell press device (Figure 9b) consists of three steel plates attached to or guided by four columns and two isolators. A central spindle connects the middle and upper plates. A hexagon nut is located on the spindle. After the cell has been inserted, a defined force is applied using a torque wrench, thus pressing the cell between the lower and middle plates. Calibration (once inserting a load cell) and torque determination are performed analogously to the first device. Finally, the hexagon nut is turned upward to prevent relaxation. The disadvantages of this design are the higher costs and larger dimensions. The advantages are central application of the force, homogeneous pressure distribution, as well as easy handling. Examples of use are the publications of Batzer et al.[59] and those of the Janek group.[59,119,135]

The last cell press device (Figure 9c) is similar to the second, but additionally has a measuring device for dynamic determination of the pressure. If a load cell is used, an additional movable plate is required; if a thin-film sensor is used, it can simply be inserted into the lower plate. The force is still applied via the spindle, the pressure is measured simultaneously after specifying the area and recorded digitally. Further calculations or calibrations are not required. The disadvantage compared to the second device are the considerable costs of the pressure

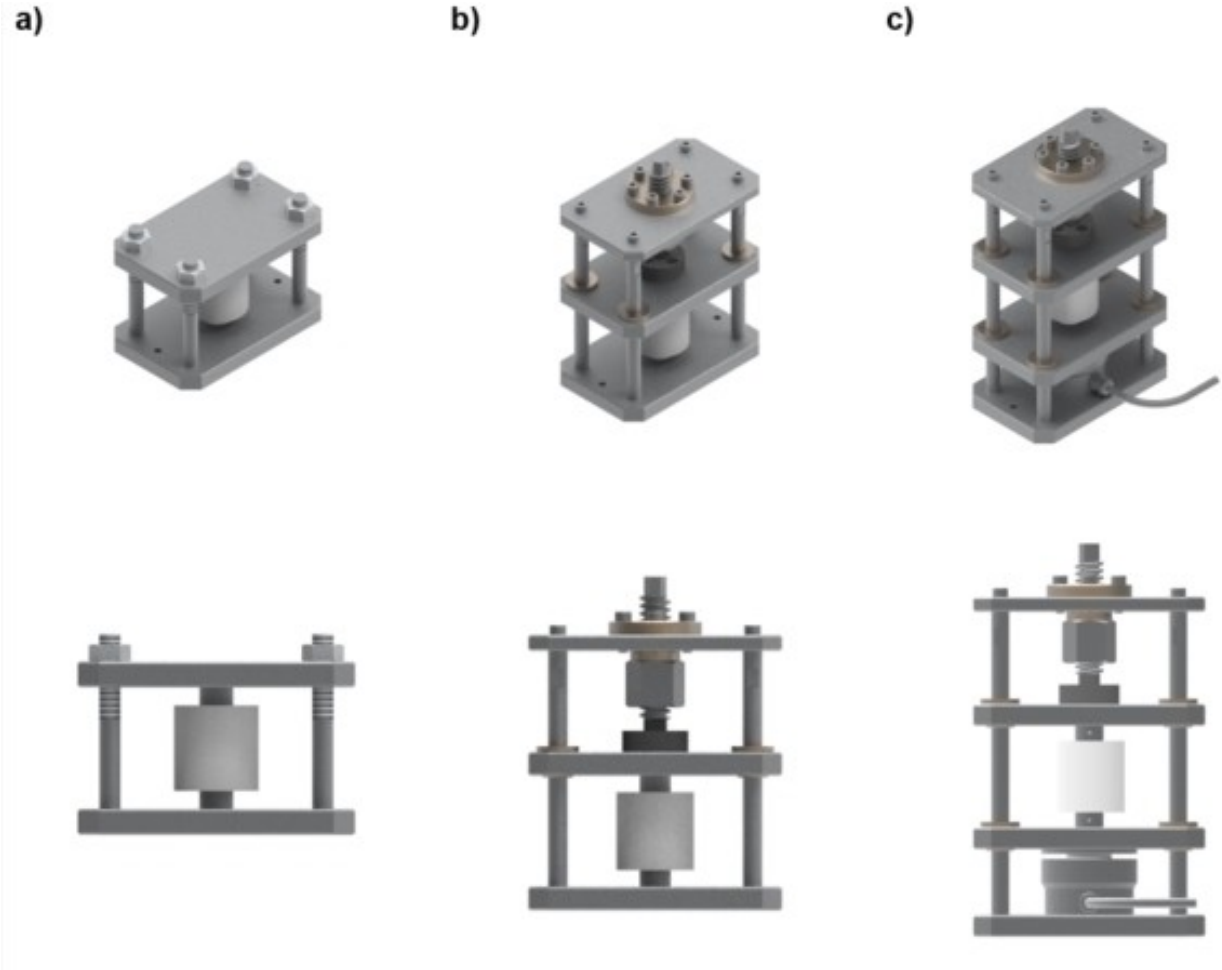

Figure 9. Isometric and frontal view of a cell press device with a) external application of pressure and release by tightening four screws, b) application of a defined torque to a central screw (previously calibrated) by torque handle, c) application of a defined torque to a central screw (dynamic pressure measurement) by torque handle.

measurement plus periphery, the advantage is the exact adjustment possibilities, as well as the observation of the pressure course during an electrochemical measurement. A load cell was also used in the device of Doux et al.[19,134]

4. Scale-up

After considering a range of procedural manufacturing processes, the approaches identified as scalable are compared with technologies already established in the field of conventional LIBs. An evaluation aiming at the production of sulfidic SSBs on an industrial level in line with the process chain shown in Figure 10 is carried out.

4.1. Synthesis

In mechanochemical synthesis, especially planetary ball mills promise reproducible material properties and acceptable

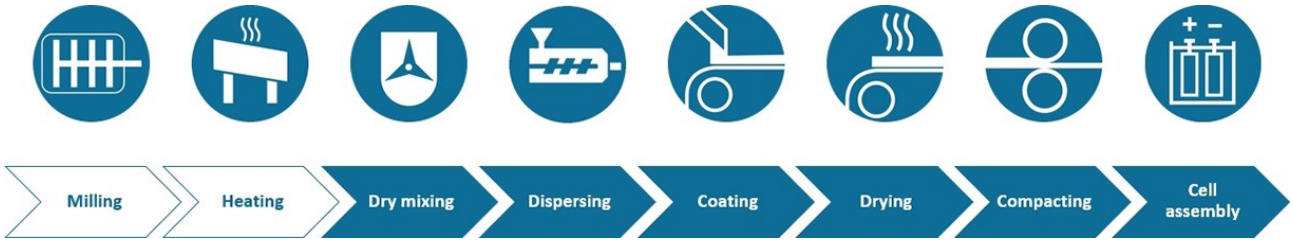

Figure 10. Process chain for the production of sulfidic SSBs on an industrial scale from dry mixing to cell construction plus mechanochemical SE synthesis

amounts of SE.[34,83,90] The consideration of different synthesis procedures shows that it is very difficult to make a general and product-independent recommendation for the parameters of the mechanochemical process. In terms of product yield, risk of contamination and stress energy, large grinding media made of an electrically insulating material with high density should be selected. Grinding media and powder fill ratio should be between 0.3 and 0.5 respectively 0.5 and 1. Large grinding chambers with a likewise electrically insulating wall are preferable. High speeds promote the energy input for the comminution and conversion of the reactants (see Section 3.1. Synthesis).[90] Regardless, they must be replaced, since they can neither be operated continuously nor built on a larger scale. This can be addressed using stirred media ball mills: Mostly employed for nano comminution, these machines have been intensively investigated and already applied in battery process technology for grinding silicon.[136] As a second synthesis step, heat treatment turned out to be advantageous to improve the ionic conductivity.[7,22,24,26,36] Due to the limited data available, no specific recommendations can be made for the duration and temperature of the heat treatment: The only variation with remaining parameters constant indicates that the ionic conductivity increases with the length and intensity of the heat treatment.[36] Although a comparison with LIBs lacks due to a lack of applications, a transfer of continuously operable circular tube furnaces from pyrolysis technology would be conceivable.[137] Due to the moisture-sensitive properties of the sulfidic solid electrolytes and part of their reactants, the synthesis must necessarily be carried out under inert gas or dry room atmospheres.

4.2. Electrode and separator processing

Both dry and wet mixing are elementary for dispersing underlying particulate components and producing a suspension with coatable viscosity: Whereas dry premixing using a mortar and pestle on a laboratory scale has already shown very good results for cathodes of sulfidic SSBs,[72] scaling up to larger plants such as drum, intensive or planetary mixers is essential.[124,138,139] Studies on LIBs already confirm, mixing intensity, as well as time can strongly affect the resulting electrode properties and cell performance.[124,125,140] For example, too intense mixing can prevent the formation of a beneficial carbon black/binder network within the electrode[124] and too gentle mixing may result in a poor structure of the conductive additive. This is also expected for sulfide-based electrodes. According to an appropriate cathode formulation for scale up, NCM is the most promising candidate as active material. Here, a small particle size[58] and high nickel content of $\times 0.8$ due to material costs as well as capacity[57] should be used. As electrolyte, agyrodites seem to be recommendable for an industrial production under consideration of material costs and ionic conductivity. With respect to electrochemical performance, as little binder as well as conductive additive as possible should be included.[59] Small sized conductive additives like VGCF should be preferred (see Section 3.2. Formulation).[52] Moreover, in consideration of economic aspects at least 70 wt% of solids content of the electrode and separator slurries have to be achieved. To our knowledge, pouch cells with sulfide-based electrolyte are yet only realized by composite anodes.[11,111] In future, the application of lithium metal as anode has to be driven forward in terms of, for example, appropriate coatings.

The subsequent wet dispersion step of cathode, as well as separator suspensions has often been carried out with PCMs so far,[11,35,97] which are limited both technically in their ability for breaking up agglomerates and economically in product volume.[122] In order to realize an industrially relevant production of sulfidic SSBs, more shear-intensive aggregates available on a large scale, such as dissolvers, kneaders, planetary mixers and twin-screw extruders,[125] have to be used. Dissolvers have already been successfully applied for dispersing suspensions and following coating of layer-based sulfide separators and cathodes, confirming the possibility of scalable implementation of the dispersion process. It has been shown that a two-stage dispersion process consisting of a single dispersion step of the powders (960 min^{-1}, 30 min) and a main dispersion step (2870 min^{-1}, 60 min) to distribute the agglomerates is beneficial[59] (see Section 3.3.1. Dispersing). The effects of sulfide solid electrolytes with different particle sizes were shown on both the dispersion process and the resulting coatings: Whereas more solvent is required for fine solid electrolytes due to the higher specific surface area, advantages result from a more homogeneous dispersion and thus better ionic connection of the active material particles, especially in the production of cathodes.[59] Twin-screw extruders are established and investigated in the field of LIBs.[127] With a mass flow rate of up to 100 t/h[141] these machines are highly relevant for industrial use and probably the future approach for an effective dispersion of sulfide-based electrode and separator slurries. In particular, the ductile character of sulfide-based electrolytes promises a good processability during the extrusion process and the possibility to significantly reduce the solvent amount[127] and result in highly homogeneous electrode and separator layers.

The film applicators used on a laboratory scale and the associated doctor blade technique[11,16,59] are transferable to continuous coating lines, which are currently established for LIBs in principle: Besides coating via comma bar or slot die technology onto the current collector (composite cathode/anode) or an electrode/carrier substrate (separator), immediate drying is possible.[1] With regard to drying temperature and technique (infrared, vacuum, convection or diffusion) and residence time, various application profiles are possible. Here, the particle size as well as the layer thickness have a significant impact on the drying performance of the cathode and separator layers. For thick layers and small sized particles milder drying procedures have to be applied to prevent the formation of cracks caused by rapid solvent evaporation (see Section 3.3.2. Wet coating and drying). Moreover, the post-drying step would be carried out similar to conventional LIB.[142] Although no work has been done to date on the production of sulfidic SSBs using continuous coating and drying equipment, their size requires special consideration of the issues described in Section 2 Challenges of sulfidic electrolytes.

To realize a continuous densification, calendering by a two-roll calender has to be established (see Figure 11).[1] One study already reports a calendering at 60 °C of sealed separator sheets outside the glovebox. They have reduced the gap size until the pouch bag curled up but without mentioning the exact line load or gap width (see Table 8, Section 3.3.3. Densification).[74] However, in future applications separators, composite cathodes and anodes probably are calendered directly after the drying process and before cutting and cell assembly. Here, various impact parameters like roll temperature, calendering speed and line load like they have been evaluated for conventional electrodes should be investigated.[143,144] One important knowledge here, for example, is that wrinkling of the electrodes can be prevented by heated calender rolls.[78] This behavior can also be expected for sulfide-bases electrodes. To achieve a low porosity within the composite electrodes and separators, which should be ideally zero percent, possibly higher line loads in comparison to those applied for conventional composite electrodes are necessary.[1]

The entire processing should be realized in dry room atmosphere to allow a continuous processing making further material engineering necessary to reduce the moisture sensibility of the electrolyte.

4.3. Cell assembly

While cutting and punching out electrode/separator sheets and using cell pressing equipment are suitable for laboratory scale, other techniques may be required for automated, large-scale industrial production and implementation in electric vehicles. The alignment to the process chain of LIBs is only possible to a limited extent in this Section, since some steps have to be added or omitted. Starting with cutting out electrode-separator-composites, Schnell et al. mention the risk of short circuits set off by conducting particles become detached while handling the components. As additional challenges they point out the precise automated and damage-free deposit stacking of the layers. Further difficulties are resulting from use of metallic lithium (stacking, welding).[1] Concluding, an intense contact between the different components has must be ensured to reduce the interfacial resistance. During manufacturing this might be possible by calendering, during operation light cell press devices are necessary. Moreover, in contrast to conventional LIBs multi-layer pouch cells in bipolar order could be realized for SSBs under the achievement of an enhanced energy density and a reduction of necessary contacting of the current collectors.[145,146] According to Jung et al., the current collector acts both as positive and negative pole, unit cells do not have to be packed and sealed individually and cell modules can be achieved by sequentially stacking or laminating of the cathode, current collector, anode and separator without external wiring.[146]

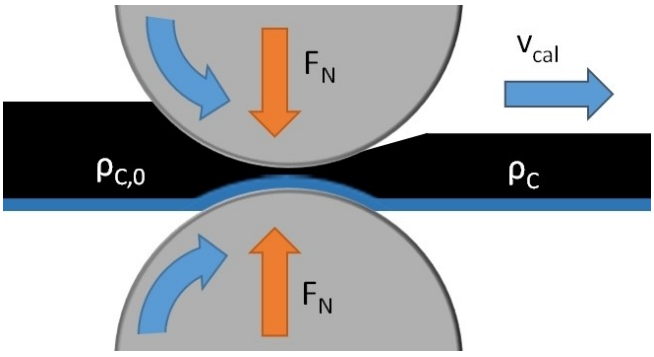

Figure 11. Calendering process. $\rho_{c,0}$ refers to the initial coating density and ρ_c to the processed coating density according to Meyer et al.[143] Adapted with permission from Ref. [143]. Copyright (2017) Elsevier.

While this publication is limited to sulfidic SEs and focuses on the process engineering implementation of the steps from synthesis to calendering, the works of Schnell et al.,[1] Duffner et al.[147] and Tan et al.[148] are recommended for the study of alternative SSB concepts, as well as economic perspectives.

5. Conclusion

Consideration of the currently used methods and processes for the production of sulfidic SSBs reveals great research and development potential, especially with regard to scaling of production to industrially relevant scale and process optimization.

Although material investigations have already been carried out using powder cells and a transfer to suspension-based processes was performed, small non-scalable laboratory equipment is mainly used (e.g., planetary centrifugal mixers). Despite the particular challenges of sulfide SEs, there is a large intersection between continuously implementable processes which are already established in the field of LIBs and the requirements of SSBs. A transfer of small-scale processes and process parameters that can only be implemented on a laboratory scale to continuous, well scalable processes and equipment is desirable.

Regardless their proven influence on the properties of battery components, the process parameters in the production of sulfidic SSBs are often incompletely specified or not mentioned at all. This is demonstrated in the synthesis of sulfidic SEs, where an increase in product quality and process efficiency is possible by considering the fundamentals of comminution technology. Analogous to the procedure for the optimization of LIBs, a modeling of process technologies is recommended.

Acknowledgements

The authors thank the European Union (EU) for the financial support of the H2020 research and innovation programme under GA Agreement no. 875028 as well as the German Federal Ministry of Education and Research (BMBF, BiSSFest – 03XP0412A) and our cooperating partners for their collaboration. Furthermore, we sincerely thank Christine Burmeister, Jannes Müller, Jeroen Volbeda, Kevin Voges and Sinem Elma for their valuable comments, discussions and contributions to the review article. Open Access funding enabled and organized by Projekt DEAL.

Appendix

Abbreviation	Subclass	Meaning
WIP	Aggregate	Warm isostatic press
GP	Anode active material	Graphite
Si	Anode active material	Silicon
LIB	Batteries	Lithium-ion battery
SSB	Batteries	Solid-state battery
CAM	Battery components	Cathode active material
SE	Battery components	Solid electrolyte
AC	Binder	Acrylate
HNBR	Binder	Hydrated nitrile butadiene rubber
NBR	Binder	Nitrile butadiene rubber
PEVA	Binder	Poly ethylene vinyl acetate
PIB	Binder	Polyisobutylene
PPC	Binder	Poly propylene carbonate
PTFE	Binder, Substrate	Polytetrafluoroethylene
SBS	Binder	Styrene butadiene styrene
SEBS	Binder	Styrene ethylene butylene styrene
NCM 111	Cathode active material	$LiNi_{1/3}Mn_{1/3}Co_{1/3}O_2$
NCM 622	Cathode active material	$LiNi_{0.6}Mn_{0.2}Co_{0.2}O_2$
NCM 811	Cathode active material	$LiNi_{0.8}Mn_{0.1}Co_{0.1}O_2$
NCM 955	Cathode active material	$LiNi_{0.9}Mn_{0.05}Co_{0.05}O_2$
AB	Conductive additive	Acetylene black
CNF	Conductive additive	Carbon nanofibers
DB	Conductive additive	Denka black
C65	Conductive additive	Super C65
VGCF	Conductive additive	Vapor grown carbon fibers
LPS	Solid electrolyte	Li_3PS_4
LPSCl	Solid electrolyte	Li_6PS_5Cl

Abbreviation	Subclass	Meaning
LPSI	Solid electrolyte	Li_6PS_5I
LSPS	Solid electrolyte	$Li_{10}SnP_2S_{12}$
IBIB	Solvent	Isobutyl isobutyrate
NMP	Solvent	N-methylpyrrolidon
PE	Substrate	Polyethylene
SUS	Substrate	Stainless steele

Conflict of Interest

The authors declare that they have no known competing financial interests or personal relationships that could have appeared to influence the work reported in this paper.

Data Availability Statement

Data sharing is not applicable to this article as no new data were created or analyzed in this study.

Keywords: Batteries · Electrode materials · Electrodes · Electrolytes · Energy storage

[1] J. Schnell, T. Günther, T. Knoche, C. Vieider, L. Köhler, A. Just, M. Keller, S. Passerini, G. Reinhart, *J. Power Sources* **2018**, *382*, 160–175.
[2] M. M. Thackeray, C. Wolverton, E. D. Isaacs, *Energy Environ. Sci.* **2012**, *5*, 7854.
[3] E. P. Roth, C. J. Orendorff, *Electrochem. Soc. Interface* **2012**, *21*, 45–49.
[4] Y.-C. Jung, S.-K. Kim, M.-S. Kim, J.-H. Lee, M.-S. Han, D.-H. Kim, W.-C. Shin, M. Ue, D.-W. Kim, *J. Power Sources* **2015**, *293*, 675–683.
[5] M. Tatsumisago, M. Nagao, A. Hayashi, *J. Asian Ceram. Soc.* **2013**, *1*, 17–25.
[6] H. Akitoshi, T. Masahiro, *Electron. Mater. Lett.* **2012**, *8*, 199–207.
[7] S. Atsushi, K. Hirokazu, H. Akitoshi, T. Kiyoharu, T. Masahiro, *J. Electrochem. Soc.* **2009**, *156*, 27–32.
[8] L. Helmers, L. Froböse, K. Friedrich, M. Steffens, D. Kern, P. Michalowski, A. Kwade, *Energy Technol.* **2021**, *9*, 2000923.
[9] Y. S. Jung, D. Y. Oh, Y. J. Nam, K. H. Park, *Isr. J. Chem.* **2015**, *55*, 472–485.
[10] Z. Gao, H. Sun, L. Fu, F. Ye, Y. Zhang, W. Luo, Y. Huang, *Adv. Mater.* **2018**, *30*, e1705702.
[11] Y.-G. Lee, S. Fujiki, C. Jung, N. Suzuki, N. Yashiro, R. Omoda, D.-S. Ko, T. Shiratsuchi, T. Sugimoto, S. Ryu, et al., *Nat. Energy* **2020**, *5*, 299–308.
[12] J. Janek, W. G. Zeier, *Nat. Energy* **2016**, *1*, 1167.
[13] J. Li, C. Ma, M. Chi, C. Liang, N. J. Dudney, *Adv. Energy Mater.* **2015**, *5*, 1401408.
[14] K. Yo, M. Hajime, T. Katsuhito, S. Hikari, T. Mitsuhara, K. Hiroyuki, I. Toru, *J. Electrochem. Soc.* **2003**, *150*, 1577–1582.
[15] F. Mizuno, C. Yada, H. Iba, *Lithium-Ion Batteries* **2014**, *57*, 273–291.
[16] K. Lee, S. Kim, J. Park, S. H. Park, A. Coskun, D. S. Jung, W. Cho, J. W. Choi, *J. Electrochem. Soc.* **2017**, *164*, A2075–A2081.
[17] S. Ohno, W. G. Zeier, *Acc. Mater. Res.* **2021**, *2*, 869–880.
[18] Z. Ma, H.-G. Xue, S.-P. Guo, *J. Mater. Sci.* **2018**, *53*, 3927–3938.
[19] J.-M. Doux, Y. Yang, D. H. S. Tan, H. Nguyen, E. A. Wu, X. Wang, A. Banerjee, Y. S. Meng, *J. Mater. Chem. A* **2020**, *8*, 5049–5055.
[20] S. Ohno, T. Bernges, J. Buchheim, M. Duchardt, A.-K. Hatz, M. A. Kraft, H. Kwak, A. L. Santhosha, Z. Liu, N. Minafra, et al., *ACS Energy Lett.* **2020**, *5*, 910–915.
[21] P. Zhou, J. Wang, F. Cheng, F. Li, J. Chen, *Chem. Commun. (Camb.)* **2016**, *52*, 6091–6094.
[22] H. Yamane, M. Shibata, Y. Shimane, T. Junke, Y. Seino, S. Adams, K. Minami, A. Hayashi, M. Tatsumisago, *Solid State Ionics* **2007**, *178*, 1163–1167.
[23] K. Minami, A. Hayashi, M. Tatsumisago, *J. Am. Ceram. Soc.* **2011**, *94*, 1779–1783.
[24] B. R. Shin, Y. J. Nam, D. Y. Oh, D. H. Kim, J. W. Kim, Y. S. Jung, *Electrochim. Acta* **2014**, *146*, 395–402.
[25] N. Kamaya, K. Homma, Y. Yamakawa, M. Hirayama, R. Kanno, M. Yonemura, T. Kamiyama, Y. Kato, S. Hama, K. Kawamoto, et al., *Nat. Mater.* **2011**, *10*, 682–686.
[26] S. Boulineau, M. Courty, J.-M. Tarascon, V. Viallet, *Solid State Ionics* **2012**, *221*, 1–5.
[27] P. R. Rayavarapu, N. Sharma, V. K. Peterson, S. Adams, *J. Solid State Electrochem.* **2012**, *16*, 1807–1813.
[28] J. Zhang, L. Li, C. Zheng, Y. Xia, Y. Gan, H. Huang, C. Liang, X. He, X. Tao, W. Zhang, *ACS Appl. Mater. Interfaces* **2020**, *12*, 41538–41545.
[29] C. Yu, J. Hageman, S. Ganapathy, L. van Eijck, L. Zhang, K. R. Adair, X. Sun, M. Wagemaker, *J. Mater. Chem. A* **2019**, *7*, 10412–10421.
[30] J. A. Brant, D. M. Massi, N. A. W. Holzwarth, J. H. MacNeil, A. P. Douvalis, T. Bakas, S. W. Martin, M. D. Gross, J. A. Aitken, *Chem. Mater.* **2015**, *27*, 189–196.
[31] T. Kaib, S. Haddadpour, M. Kapitein, P. Bron, C. Schröder, H. Eckert, B. Roling, S. Dehnen, *Chem. Mater.* **2012**, *24*, 2211–2219.
[32] R. Matsuda, T. Kokubo, N. H. H. Phuc, H. Muto, A. Matsuda, *Solid State Ionics* **2020**, *345*, 115190.
[33] H. Morimoto, H. Yamashita, M. Tatsumisago, T. Minami, *J. Am. Ceram. Soc.* **1999**, *82*, 1352–1354.
[34] A. Hayashi, S. Hama, H. Morimoto, M. Tatsumisago, T. Minami, *J. Am. Ceram. Soc.* **2001**, *84*, 477–479.
[35] A. Sakuda, K. Kuratani, M. Yamamoto, M. Takahashi, T. Takeuchi, H. Kobayashi, *J. Electrochem. Soc.* **2017**, *164*, A2474.
[36] J. Kim, M. Eom, S. Noh, D. Shin, *Electron. Mater. Lett.* **2012**, *8*, 209–213.
[37] Y. Zhang, R. Chen, T. Liu, Y. Shen, Y. Lin, C.-W. Nan, *ACS Appl. Mater. Interfaces* **2017**, *9*, 28542–28548.
[38] P. Bron, S. Johansson, K. Zick, J. Schmedt auf der Günne, S. Dehnen, B. Roling, *J. Am. Chem. Soc.* **2013**, *135*, 15694–15697.
[39] A. Kuhn, O. Gerbig, C. Zhu, F. Falkenberga, J. Maier, B. V. Lotsch, *Phys. Chem. Chem. Phys.* **2014**, *16*, 14669–14674.
[40] C. Lovatt Evans, *Quart. J. exp. Physiol.* **1967**, *52*, 231–248.
[41] T. L. Guidotti, *Occup. Med.* **1996**, *46*, 367–371.
[42] D. S. Chamberlin, D. R. Clarke, *Ind. Eng. Chem.* **1928**, *20*, 1016–1018.
[43] C. Singer, H.-C. Töpper, T. Kutsch, R. Schuster, R. Koerver, R. Daub, *ACS Appl. Mater. Interfaces* **2022**, *14*, 24245–24254.
[44] M. Calpa, N. C. Rosero-Navarro, A. Miura, R. Jalem, Y. Tateyama, K. Tadanaga, *Appl. Mater.Today* **2021**, *22*, 100918.
[45] L. Peng, S. Chen, C. Yu, C. Wei, C. Liao, Z. Wu, H.-L. Wang, S. Cheng, J. Xie, *ACS Appl. Mater. Interfaces* **2022**, *14*, 4179–4185.
[46] S. Ito, S. Fujiki, T. Yamada, Y. Aihara, Y. Park, T. Y. Kim, S.-W. Baek, J.-M. Lee, S. Doo, N. Machida, *J. Power Sources* **2014**, *248*, 943–950.
[47] J. Lee, T. Lee, K. Char, K. J. Kim, J. W. Choi, *Acc. Chem. Res.* **2021**, *54*, 3390–3402.

[48] H. Muramatsu, A. Hayashi, T. Ohtomo, S. Hama, M. Tatsumisago, *Solid State Ionics* **2011**, *182*, 116–119.
[49] T. Kimura, A. Kato, C. Hotehama, A. Sakuda, A. Hayashi, M. Tatsumisago, *Solid State Ionics* **2019**, *333*, 45–49.
[50] A. Hayashi, H. Muramatsu, T. Ohtomo, S. Hama, M. Tatsumisago, *J. Mater. Chem. A* **2013**, *1*, 6320.
[51] T. Bartsch, F. Strauss, T. Hatsukade, A. Schiele, A.-Y. Kim, P. Hartmann, J. Janek, T. Brezesinski, *ACS Energy Lett.* **2018**, *3*, 2539–2543.
[52] F. Walther, S. Randau, Y. Schneider J Sann, M. Rohnke, F. H. Richter, W. G. Zeier, J. Janek, *Chem. Mater.* **2020**, *32*, 6123–6136.
[53] R. Koerver, W. Zhang, L. de Biasi, S. Schweidler, A. O. Kondrakov, S. Kolling, T. Brezesinski, P. Hartmann, W. G. Zeier, J. Janek, *Energy Environ. Sci.* **2018**, *11*, 2142–2158.
[54] R. Koerver, I. Aygün, T. Leichtweiß, C. Dietrich, W. Zhang, J. O. Binder, P. Hartmann, W. G. Zeier, J. Janek, *Chem. Mater.* **2017**, *29*, 5574–5582.
[55] J. N. Reimers, J. R. Dahn, *J. Electrochem. Soc.* **1992**, *139*, 2091.
[56] F. Strauss, L. de Biasi, A.-Y. Kim, J. Hertle, S. Schweidler, J. Janek, P. Hartmann, T. Brezesinski, *ACS Materials Lett.* **2020**, *2*, 84–88.
[57] C. A. Heck, M.-W. von Horstig, F. Huttner, J. K. Mayer, W. Haselrieder, A. Kwade, *J. Electrochem. Soc.* **2020**, *167*, 160521.
[58] F. Strauss, T. Bartsch, L. de Biasi, A.-Y. Kim, J. Janek, P. Hartmann, T. Brezesinski, *ACS Energy Lett.* **2018**, *3*, 992–996.
[59] M. Batzer, K. Voges, W. Wang, P. Michalowski, A. Kwade, *Mater. Today Commun.* **2022**, *30*, 103189.
[60] H.-H. Ryu, K.-J. Park, C. S. Yoon, Y.-K. Sun, *Chem. Mater.* **2018**, *30*, 1155–1163.
[61] S. S. Zhang, *Energy Storage Mater.* **2020**, *24*, 247–254.
[62] S. Wenzel, T. Leichtweiss, D. Krüger, J. Sann, J. Janek, *Solid State Ionics* **2015**, *278*, 98–105.
[63] S. Wenzel, D. A. Weber, T. Leichtweiss, M. R. Busche, J. Sann, J. Janek, *Solid State Ionics* **2016**, *286*, 24–33.
[64] K. J. Kim, M. Balaish, M. Wadaguchi, L. Kong, J. L. M. Rupp, *Adv. Energy Mater.* **2021**, *11*, 2002689.
[65] Y. Yang, Q. Wu, Y. Cui, Y. Chen, S. Shi, R.-Z. Wang, H. Yan, *ACS Appl. Mater. Interfaces* **2016**, *8*, 25229–25242.
[66] R. Koerver, F. Walther, I. Aygün, J. Sann, C. Dietrich, W. G. Zeier, J. Janek, *J. Mater. Chem. A* **2017**, *5*, 22750–22760.
[67] X. Zhang, Q. J. Wang, K. L. Harrison, S. A. Roberts, S. J. Harris, *Cell Rep. Phy. Science* **2020**, *1*, 100012.
[68] M. J. Wang, R. Choudhury, J. Sakamoto, *Joule* **2019**, *3*, 2165–2178.
[69] Y. Pang, J. Pan, J. Yang, S. Zheng, C. Wang, *Electrochem. Energy Rev.* **2021**, *4*, 169–193.
[70] S. Wang, R. Fang, Y. Li, Y. Liu, C. Xin, F. H. Richter, C.-W. Nan, *J. Materiomics* **2021**, *7*, 209–218.
[71] A. Gurung, J. Pokharel, A. Baniya, R. Pathak, K. Chen, B. S. Lamsal, N. Ghimire, W.-H. Zhang, Y. Zhou, Q. Qiao, *Sustain. Energy Fuels* **2019**, *3*, 3279–3309.
[72] S. Noh, W. T. Nichols, M. Cho, D. Shin, *J. Electroceram.* **2018**, *40*, 293–299.
[73] S. Atsushi, H. Akitoshi, T. Masahiro, *Sci. Rep.* **2013**, *3*, 2261.
[74] N. Riphaus, P. Strobl, B. Stiaszny, T. Zinkevich, M. Yavuz, J. Schnell, S. Indris, H. A. Gasteiger, S. J. Sedlmaier, *J. Electrochem. Soc.* **2018**, *165*, 3993–3999.
[75] N. C. Rosero-Navarro, T. Kinoshita, A. Miura, M. Higuchi, K. Tadanaga, *Ionics* **2017**, *23*, 1619–1624.
[76] S. Troy, A. Schreiber, T. Reppert, H.-G. Gehrke, M. Finsterbusch, S. Uhlenbruck, P. Stenzel, *Appl. Energy* **2016**, *169*, 757–767.
[77] C. Yu, S. Ganapathy, J. Hageman, L. van Eijck, E. R. H. van Eck, L. Zhang, T. Schwietert, S. Basak, E. M. Kelder, M. Wagemaker, *ACS Appl. Mater. Interfaces* **2018**, *10*, 33296–33306.
[78] A. Kwade, W. Haselrieder, R. Leithoff, A. Modlinger, F. Dietrich, K. Droeder, *Nat. Energy* **2018**, *3*, 290–300.
[79] D. H. S. Tan, P. Xu, H. Yang, M.-c. Kim, H. Nguyen, E. A. Wu, J.-M. Doux, A. Banerjee, Y. S. Meng, Z. Chen, *MRS Energy Sustainability* **2020**, *7*, 375.
[80] S. Doose, J. K. Mayer, P. Michalowski, A. Kwade, *Metals* **2021**, *11*, 291.
[81] M. Schubert, D. Hanft, T. Nazarenus, J. Exner, M. Schubert, P. Nieke, P. Glosse, N. Leupold, J. Kita, R. Moos, *Funct. Mater. Lett.* **2019**, *12*, 1930005.
[82] S. Tschöcke, H. Altuhues, B. Schumm, S. Kaskel, C. Schult, D. Fritsche, K. Schönherr, *Patent* **2018**, *DE102017208220A1*, Deutsches Patent- und Markenamt, https://register.dpma.de/DPMAregister/pat/register?AKZ=1020172082208&CURSOR=0 .
[83] J. Wu, S. Liu, F. Han, X. Yao, C. Wang, *Adv. Mater.* **2021**, *33*, e2000751.
[84] Ö. U. Kudu, T. Famprikis, B. Fleutot, M.-D. Braida, T. Le Mercier, M. S. Islam, C. Masquelier, *J. Power Sources* **2018**, *407*, 31–43.
[85] K. Homma, M. Yonemura, T. Kobayashi, M. Nagao, M. Hirayama, R. Kanno, *Solid State Ionics* **2011**, *182*, 53–58.
[86] C. Yu, S. Ganapathy, N. J. J. de Klerk, I. Roslon, E. R. H. van Eck, A. P. M. Kentgens, M. Wagemaker, *J. Am. Chem. Soc.* **2016**, *138*, 11192–11201.
[87] S. Ito, M. Nakakita, Y. Aihara, T. Uehara, N. Machida, *J. Power Sources* **2014**, *271*, 342–345.
[88] S. Yubuchi, S. Teragawa, K. Aso, K. Tadanaga, A. Hayashi, M. Tatsumisago, *J. Power Sources* **2015**, *293*, 941–945.
[89] L. Zhou, K.-H. Park, X. Sun, F. Lalère, T. Adermann, P. Hartmann, L. F. Nazar, *ACS Energy Lett.* **2019**, *4*, 265–270.
[90] R. Schlem, C. F. Burmeister, P. Michalowski, S. Ohno, G. F. Dewald, A. Kwade, W. G. Zeier, *Adv. Energy Mater.* **2021**, *11*, 2101022.
[91] S. Randau, D. A. Weber, O. Kötz, R. Koerver, P. Braun, A. Weber, E. Ivers-Tiffée, T. Adermann, J. Kulisch, W. G. Zeier, et al., *Nat. Energy* **2020**, *5*, 259–270.
[92] S. P. Culver, R. Koerver, W. G. Zeier, J. Janek, *Adv. Energy Mater.* **2019**, *9*, 1900626.
[93] H. Lee, P. Oh, J. Kim, H. Cha, S. Chae, S. Lee, J. Cho, *Adv. Mater.* **2019**, *31*, e1900376.
[94] K. Takada, N. Ohta, L. Zhang, X. Xu, B. T. Hang, T. Ohnishi, M. Osada, T. Sasaki, *Solid State Ionics* **2012**, *225*, 594–597.
[95] F. Walther, F. Strauss, X. Wu, B. Mogwitz, J. Hertle, J. Sann, M. Rohnke, T. Brezesinski, J. Janek, *Chem. Mater.* **2021**, *33*, 2110–2125.
[96] Y.-J. Kim, R. Rajagopal, S. Kang, K.-S. Ryu, *Chem. Eng. J.* **2020**, *386*, 123975.
[97] M. Yamamoto, M. Takahashi, Y. Terauchi, Y. Kobayashi, S. Ikeda, A. Sakuda, *J. Ceram. Soc. Jpn.* **2017**, *125*, 391–395.
[98] A. Bielefeld, D. A. Weber, J. Janek, *ACS Appl. Mater. Interfaces* **2020**, *12*, 12821–12833.
[99] A. Bielefeld, D. A. Weber, J. Janek, *J. Phys. Chem. C* **2019**, *123*, 1626–1634.
[100] T. Shi, Q. Tu, Y. Tian, Y. Xiao, L. J. Miara, O. Kononova, G. Ceder, *Adv. Energy Mater.* **2020**, *10*, 1902881.
[101] C. Park, S. Lee, K. Kim, M. Kim, S. Choi, D. Shin, *J. Electrochem. Soc.* **2019**, *166*, A5318–A5322.
[102] E. Hayakawa, H. Nakamura, S. Ohsaki, S. Watano, *Adv. Powder Technol.* **2022**, *33*, 103470.
[103] Y. Han, S. H. Jung, H. Kwak, S. Jun, H. H. Kwak, J. H. Lee, S.-T. Hong, Y. S. Jung, *Adv. Energy Mater.* **2021**, *11*, 2100126.
[104] F. Huttner, A. Diener, T. Heckmann, J. C. Eser, T. Abali, J. K. Mayer, P. Scharfer, W. Schabel, A. Kwade, *J. Electrochem. Soc.* **2021**, *168*, 90539.
[105] W. Zhang, T. Leichtweiß, S. P. Culver, R. Koerver, D. Das, D. A. Weber, W. G. Zeier, J. Janek, *ACS Appl. Mater. Interfaces* **2017**, *9*, 35888–35896.
[106] Y.-H. Chen, C.-W. Wang, X. Zhang, A. M. Sastry, *J. Power Sources* **2010**, *195*, 2851–2862.
[107] B. J. Landi, M. J. Ganter, C. D. Cress, R. A. DiLeo, R. P. Raffaelle, *Energy Environ. Sci.* **2009**, *2*, 638.
[108] S. Hong, J. Kim, M. Kim, X. Meng, G. Lee, D. Shin, *Ceram. Int.* **2015**, *41*, 5066–5071.
[109] S. Toyokuni, *Adv. Drug Delivery Rev.* **2013**, *65*, 2098–2110.
[110] M. Ménétrier, I. Saadoune, S. Levsseur, C. Delmas, *J. Mater. Chem.* **1999**, *9*, 1135–1140.
[111] Y. J. Nam, D. Y. Oh, S. H. Jung, Y. S. Jung, *J. Power Sources* **2018**, *375*, 93–101.
[112] T. Ates, M. Keller, J. Kulisch, T. Adermann, S. Passerini, *Energy Storage Mater.* **2019**, *17*, 204–210.
[113] M. Kroll, M. Duchardt, S. L. Karstens, S. Schlabach, F. Lange, J. Hochstrasser, B. Roling, U. Tallarek, *J. Power Sources* **2021**, *505*, 230064.
[114] D. Lin, Y. Liu, Y. Cui, *Nat. Nanotechnol.* **2017**, *12*, 194–206.
[115] X.-B. Cheng, R. Zhang, C.-Z. Zhao, Q. Zhang, *Chem. Rev.* **2017**, *117*, 10403–10473.
[116] Y. Zhu, X. He, Y. Mo, *ACS Appl. Mater. Interfaces* **2015**, *7*, 23685–23693.
[117] T. Krauskopf, F. H. Richter, W. G. Zeier, J. Janek, *Chem. Rev.* **2020**, *120*, 7745–7794.
[118] Y. Kato, S. Hori, T. Saito, K. Suzuki, M. Hirayama, A. Mitsui, M. Yonemura, H. Iba, R. Kanno, *Nat. Energy* **2016**, *1*, 652.
[119] W. Zhang, D. A. Weber, H. Weigand, T. Arlt, I. Manke, D. Schröder, R. Koerver, T. Leichtweiss, P. Hartmann, W. G. Zeier, et al., *ACS Appl. Mater. Interfaces* **2017**, *9*, 17835–17845.
[120] P. Bieker, M. Winter, *Chem. Unserer Zeit* **2016**, *50*, 26–33.
[121] S. Cangaz, F. Hippauf, F. S. Reuter, S. Doerfler, T. Abendroth, H. Althues, S. Kaskel, *Adv. Energy Mater.* **2020**, *10*, 2001320.

[122] THINKY U. S. A. INC., "Technology/What is a Planetary Centrifugal System?", can be found under https://www.thinkymixer.com/en-us/planetary-centrifugal-system/.
[123] VMA-Getzmann GmbH, "Dispersion with dissolvers/Dispersion process", can be found under https://www.vma-getzmann.com/know-how/dispersion-with-dissolvers/dispersion-process/.
[124] H. Bockholt, W. Haselrieder, A. Kwade, *ECS Trans.* **2013**, *50*, 25–35.
[125] H. Dreger, H. Bockholt, W. Haselrieder, A. Kwade, *J. Electron. Mater.* **2015**, *44*, 4434–4443.
[126] W. Haselrieder, S. Ivanov, H. Y. Tran, S. Theil, L. Froböse, B. Westphal, M. Wohlfahrt-Mehrens, A. Kwade, *Prog. Solid State Chem.* **2014**, *42*, 157–174.
[127] M. Haarmann, D. Grießl, A. Kwade, *Energy Technol.* **2021**, *9*, 2100250.
[128] J. H. Teo, F. Strauss, Đ. Tripković, S. Schweidler, Y. Ma, M. Bianchini, J. Janek, T. Brezesinski, *Cell Rep. Phys. Sci.* **2021**, *2*, 100465.
[129] B. G. Westphal, A. Kwade, *J. Energy Storage* **2018**, *18*, 509–517.
[130] L. Froboese, P. Titscher, B. Westphal, W. Haselrieder, A. Kwade, *Mater. Charact.* **2017**, *133*, 102–111.
[131] A. Hayashi, A. Sakuda, M. Tatsumisago, *Front. Energy Res.* **2016**, *4*, 35.
[132] A. Ohashi, M. Kodama, S. Xueying, S. Hori, K. Suzuki, R. Kanno, S. Hirai, *J. Power Sources* **2020**, *470*, 228437.
[133] H. Bockholt, M. Indrikova, A. Netz, F. Golks, A. Kwade, *J. Power Sources* **2016**, *325*, 140–151.
[134] J.-M. Doux, H. Nguyen, D. H. S. Tan, A. Banerjee, X. Wang, E. A. Wu, C. Jo, H. Yang, Y. S. Meng, *Adv. Energy Mater.* **2020**, *10*, 1903253.
[135] W. Zhang, F. H. Richter, S. P. Culver, T. Leichtweiss, J. G. Lozano, C. Dietrich, P. G. Bruce, W. G. Zeier, J. Janek, *ACS Appl. Mater. Interfaces* **2018**, *10*, 22226–22236.
[136] A. Kwade, M. Möller, J. Müller, J. Hesselbach, S. Zellmer, S. Doose, J. Mayer, P. Michalowski, M. Powell, S. Breitung-Faes, *Kona* **2022**, *40*..
[137] G. J. Heynderickx, G. F. Froment, *Ind. Eng. Chem. Res.* **1996**, *35*, 2183–2189.
[138] Maschinenfabrik Gustav Eirich GmbH & Co KG, "Processes/Mixing technology/Intensive mixers/DW40", can be found under https://www.eirich.com/en/processes/mixing-technology/intensive-mixers.
[139] B. G. Westphal, N. Mainusch, C. Meyer, W. Haselrieder, M. Indrikova, P. Titscher, H. Bockholt, W. Viöl, A. Kwade, *J. Energy Storage* **2017**, *11*, 76–85.
[140] H. Bockholt, W. Haselrieder, A. Kwade, *Powder Technol.* **2016**, *297*, 266–274.
[141] Coperion GmbH, "Products & Services/Extruders and Compounding Machines", can be found under https://www.coperion.com/en/products-services/extruders-compounding-machines.
[142] F. Huttner, A. Marth, J. C. Eser, T. Heckmann, J. Mohacsi, J. K. Mayer, P. Scharfer, W. Schabel, A. Kwade, *Batteries & Supercaps* **2021**, *4*, 1499–1515.
[143] C. Meyer, H. Bockholt, W. Haselrieder, A. Kwade, *J. Mater. Process. Technol.* **2017**, *249*, 172–178.
[144] C. Meyer, M. Weyhe, W. Haselrieder, A. Kwade, *Energy Technol.* **2020**, *8*, 1900175.
[145] A. Sakuda, *J. Ceram. Soc. Jpn.* **2018**, *126*, 675–683.
[146] K.-N. Jung, H.-S. Shin, M.-S. Park, J.-W. Lee, *ChemElectroChem.* **2019**, *6*, 3842–3859.
[147] F. Duffner, N. Kronemeyer, J. Tübke, J. Leker, M. Winter, R. Schmuch, *Nat. Energy* **2021**, *6*, 123–134.
[148] D. H. S. Tan, Y. S. Meng, J. Jang, *Joule* **2022**, *6*, 1755–1769.

Manuscript received: July 21, 2022
Revised manuscript received: September 6, 2022
Accepted manuscript online: September 13, 2022
Version of record online: October 27, 2022